



# Towards the systematic reconnaissance of seismic signals from glaciers and ice sheets – Part 2: Unsupervised learning for source process characterization

Rebecca B. Latto<sup>1</sup>, Ross J. Turner<sup>1</sup>, Anya M. Reading<sup>1</sup>, Sue Cook<sup>2</sup>, Bernd Kulesa<sup>3</sup>, and J. Paul Winberry<sup>4</sup>

<sup>1</sup>School of Natural Sciences (Physics), University of Tasmania, Private Bag 37, Hobart, TAS 7001, Australia

<sup>2</sup>Australian Antarctic Program Partnership, Institute for Marine and Antarctic Studies, 20 Castray Esplanade, Battery Point, TAS 7004, Australia

<sup>3</sup>Glaciology Group, College of Science, Swansea University, Singleton Park, Swansea, SA2 8PP, UK

<sup>4</sup>Department of Geological Sciences, Central Washington University, Ellensburg, WA, USA

**Correspondence:** Rebecca B. Latto (beccablatto@gmail.com)

Received: 19 June 2023 – Discussion started: 25 July 2023

Revised: 29 December 2023 – Accepted: 18 March 2024 – Published: 30 April 2024

**Abstract.** Given the high number and diversity of events in a typical cryoseismic dataset, in particular those recorded on ice sheet margins, it is desirable to use a semi-automated method of grouping similar events for reconnaissance and ongoing analysis. We present a workflow for employing semi-unsupervised cluster analysis to inform investigations of the processes occurring in glaciers and ice sheets. In this demonstration study, we make use of a seismic event catalogue previously compiled for the Whillans Ice Stream, for the 2010–2011 austral summer (outlined in Part 1, Latto et al., 2024). We address the challenges of seismic event analysis for a complex wave field by clustering similar seismic events into groups using characteristic temporal, spectral, and polarization attributes of seismic time series with the *k*-means++ algorithm. This provides the basis for a reconnaissance analysis of a seismic wave field that contains local events (from the ice stream) set in an ambient wave field that itself contains a diversity of signals (mostly from the Ross Ice Shelf). As one result, we find that two clusters include stick-slip events that diverge in terms of length and initiation locality (i.e., central sticky spot and/or the grounding line). We also identify a swarm of high-frequency signals on 16–17 January 2011 that are potentially associated with a surface melt event from the Ross Ice Shelf. Used together with the event detection presented in Part 1, the semi-automated workflow could readily be generalized to other locations and, as a possible benchmark procedure, could enable the moni-

toring of remote glaciers over time and comparisons between locations.

## 1 Introduction

Cryoseismology is a field of glaciological research motivated by the possibility of inferring aspects of glacier structure and processes from seismic signals, based on a continuous record of signals potentially from the entire volume of the glacier and its surroundings (VanWormer and Berg, 1973; Podolskiy and Walter, 2016; Aster and Winberry, 2017). The field has been enabled in recent decades by increased seismic deployments to remote locations (Kanao, 2018, Chap. 8). Networks of cryoseismic instruments present the opportunity to monitor the non-tectonic seismic waves that are generated through a number of different mechanisms in response to gravitational and thermal forcing, acting on bodies of ice. Investigating glaciers with such passive seismic methods adds to knowledge that might be generated based on data collected using in situ and satellite methods (Wiens et al., 2008; Podolskiy et al., 2018). Seismic approaches can also inform the understanding of aseismic deformation through the detection of fine differences between viscous and elastic rheologies (Podolskiy et al., 2019). The range of cryoseismic event types represents the diversity of mechanisms acting on and within a glacier. These include basal slip, meltwa-

ter flow, and brittle failure (Nath and Vaughan, 2003). As a glacier moves intermittently over the bedrock and sediments beneath, it can experience basal stick-slip, resulting in signals at low frequencies of  $10^{-2}$  Hz lasting over 20–30 min (Pratt et al., 2014). Stick-slip is a cyclical process that first responds to built-up elastic strain in sticky spots at the base and then releases that strain when lubricated by meltwater (Winberry et al., 2011). Sticky spots usually arise on frozen ground where there is insufficient water to decouple the glacier from the bed. Lubrication can come from englacial drainage pathways or regelation, which is defined as the melt response to high contact pressures.

Meltwater flow can trigger a number of seismic responses from a glacier; examples include water flow that results in fluid-induced resonance (Benn et al., 2009; Hammer et al., 2015) and changing water pressure resulting in crack opening or propagation (see Table S3 in the Supplement; Colgan et al., 2016). As examples of such diverse signal types, the filling and draining of hydrological pathways (Fountain and Walder, 1998) produce relatively long, monochromatic, and harmonic seismic signals at frequencies between 1–10 Hz (Winberry et al., 2009a). In contrast, crevasse formation is a quick surface process (occurring within seconds) and generates seismic waves with frequencies between 10–100 Hz (Rööslü et al., 2014). Surface fracturing can be triggered by increasing water pressure (Carmichael et al., 2012), contraction of the ice in response to changing air temperatures (Lombardi et al., 2019), tidal bending (Cole, 2020), or horizontal stretching (Podolskiy et al., 2016; Minowa et al., 2019). Brittle deformation can also occur through the body of a glacier (Nath and Vaughan, 2003). Active processes at the downstream end of marine-terminating glaciers include basal outflow and iceberg calving, and other ocean–ice interactions can also be studied using seismic events, although they are not a focus of this study.

Glacier-focused seismic deployments typically make use of arrays of multiple sensors; therefore, it can be a time-consuming process to analyze the data recorded over many months. Visual inspection by an experienced human analyst (manual event detection) is highly informative but not suited to large data volumes. It can also result in some aspects of the resulting event catalogue being analyst dependent. A semi-automated approach is therefore desirable. The first step to automation, robust event detection, is addressed in Latto et al. (2024), which describes an algorithm designed for diverse, low-signal-to-noise microseismicity from glaciers. The next step is event analysis, where data-driven approaches present an appealing way forward (Bergen and Beroza, 2019). We use the term “event” broadly to include impulsive signals from glacier processes described above and waveform changes (such as an amplitude increase or frequency content change) with a less distinct onset that often arise in the seismic wave field.

Machine learning is a general term for the application of computer algorithms to data for the purposes of prediction

and pattern detection. It can be termed “supervised” or “unsupervised”, where supervision in this context refers to the use of labeled data to train an algorithm (Marsland, 2015). The choice of system parameterization and algorithm is dependent on the presented problem and the questions of interest. Supervised learning is often carried out using artificial neural networks to perform classification and to build predictive models (Caruana and Niculescu-Mizil, 2006; Sibi et al., 2013). Other types of supervised learning algorithms for classification purposes include random forests and support vector machines (Cracknell and Reading, 2013). Unsupervised learning algorithms are “inductive” as they develop the classification, or other model types, from properties of the data themselves, i.e., not by using a labeled training dataset. Such approaches, ranging from minimally intensive to more expensive, include  $k$ -means clustering, hierarchical methods, and self-organizing maps (Jain, 2010).

The  $k$ -means clustering algorithm ( $k$ -means) is a relatively straightforward unsupervised learning algorithm, useful for partitioning datasets into groups of similar elements, called clusters (Anderberg, 2014; George, 2013). The  $k$ -means problem aims to converge on the minimized Euclidean distance between each element to form the most well separated clusters. Before solving,  $k$ -means requires the definition of two parameters: the number of clusters and the locations of the cluster centers, called “seeds”. One challenge is that the number of clusters representative of a dataset is not known a priori. Therefore, it is useful to compute the degree of separation between clusters in order to determine how similar the  $k$ -means solutions are for a preset number of clusters (Meilä, 2006; Zadeh and Ben-David, 2009). To determine the most advantageous locations for the cluster seeds, the  $k$ -means++ algorithm has been developed as a variation of the standard algorithm, whereby cluster seeds are uniformly dispersed at locations that are spread over the data such that any two seed locations are not too near (Arthur and Vassilvitskii, 2006). Such a distribution improves  $k$ -means’ speed and accuracy because the well-separated cluster seeds can better predict well-separated clusters. The  $k$ -means++ initialization procedure is more robust than a pseudo-random seeding and less prone to user bias than a deliberate choice of seed locations.

Distance-based clustering methods like  $k$ -means can have the caveat of reduced utility in higher dimensions. The indirect relationship between dimension and utility is referred to as the curse of dimensionality in the literature (Beyer et al., 1999; Aggarwal et al., 2001);  $k$ -means is an example of a *hard* clustering algorithm where each observation is assigned to one cluster. Other clustering algorithms include the Gaussian mixture model, which is a popular alternative to  $k$ -means where each observation can belong to every cluster by means of an expectation-maximization function that produces probability distributions of cluster matches per observation (an example of *soft* clustering; Bouveyron et al., 2007). The choice of which unsupervised learning algorithm

to apply depends on the preferred solution by the user; for this work we use *k*-means as a transparent algorithm for a reconnaissance workflow and result.

Machine learning applied to earthquake seismology is advancing rapidly due to the need for automated analysis given the wealth of available data (Bergen et al., 2019). Supervised learning approaches are able to draw on access to labeled data (e.g., 1.2 million labeled seismic signal recordings; Mousavi et al., 2019). Unsupervised learning also benefits from labeled data in seismology because of the opportunity to validate and constrain results (Yoon et al., 2015; Galvis et al., 2017). Machine learning algorithms applied to seismic events often require as input the decomposition of events into attributes, called “features”, that typically describe the temporal, spectral, polarization, and network characteristics of a seismic time series (Riggelsen and Ohrberger, 2014; Reynen and Audet, 2017). Discrimination between events is improved by careful selection of the features used as input to the learning phase of algorithms (Mousavi et al., 2016).

The application of machine learning to geotechnical and environmental seismology is appealing because of the potential for the automated monitoring and classification of long, continuous, and relatively recent records (Hibert et al., 2019). Environmental seismology signals, as noted previously, can be varied in character and difficult to distinguish from ambient (i.e., background) noise because of their weak amplitude. Further, labeled datasets are less commonly developed in environmental studies. Therefore, unsupervised learning is a compelling approach for reconnaissance analysis of geotechnical and environmental seismicity records (Johnson et al., 2020). As examples, unsupervised learning has shown to be successful for classifying types of mine seismicity (e.g., *k*-means; Chamarczuk et al., 2020), discriminating between volcano-tectonic and rockfall events (e.g., self-organizing maps; Köhler et al., 2010), and clustering landslide seismicity (e.g., deep convolutional neural networks; Seydoux et al., 2020). Such machine learning applications to lower-energy signals especially benefit from the decomposition of event catalogues to datasets of features because traditional discrimination between waveforms is difficult when all events are of weak amplitude (Provost et al., 2017).

Applying machine learning to cryoseismology may enable discoveries regarding glacier dynamics and hydrological processes. Many cryoseismic signals are difficult for the human analyst or traditional methods to distinguish above background noise (e.g., Pomeroy et al., 2013). Unsupervised routines that can detect and classify events may distinguish some of the underlying processes. In terms of event discrimination, machine learning can be used to differentiate between icequakes and earthquakes without prior knowledge of the structures of the cryoseismic signals (Jenkins et al., 2021). Similar applications can also detect calving events and avalanches in continuous seismic data (Köhler et al., 2012, and Heck et al., 2018, respectively). Automated classi-

fication of cryoseismicity can enable investigation into processes which might otherwise be hidden from satellites or other in situ observations. For example, the automated detection and classification of seismic events has been used to identify an ice shelf fracture process induced by tidal bending, followed by resonance as seawater presumably fills the new fracture (Hammer et al., 2015). By studying the timing of icequake rupture, englacial meltwater flow has been related to other processes, such as heating by solar radiation and cooling induced by katabatic winds (Helmstetter et al., 2015; Sawi et al., 2022).

The aforementioned studies demonstrate that as experience builds in applying machine learning to cryoseismology, there is potential for different seasons and locations to be compared. A repeatable approach will afford the possibility of making comparisons between years for a given glacier environment and of comparing different localities. The two companion papers presented as Latto et al. (2024) (Part 1) and this work (Part 2), respectively, demonstrate a systematic workflow in (1) building a catalogue and (2) using a simple clustering method as a reconnaissance tool to better understand glacier dynamic and hydrological processes.

We first review the seismic event catalogue compiled for the Whillans Ice Stream austral summer 2010–2011 deployment. We then present and evaluate an unsupervised learning procedure, examining potential steps for constructing a dataset of informative features that capture all aspects of each seismic event while limiting biases. We implement the *k*-means++ clustering algorithm for grouping seismic events and explore *k*-means++ solutions supported by a manual appraisal of the event catalogue, investigating how the *k*-means++ solutions evolve and choosing the logical number of clusters for the analysis. In Sect. 4, we interpret the clusters in terms of probable glacier processes and noise generation mechanisms that give rise to some of the distinct groups of Whillans Ice Stream seismicity.

## 2 Whillans Ice Stream seismic event catalogue

The Whillans Ice Stream (WIS; previously known as Ice Stream B) is one of five major outlet glaciers of the Siple Coast (Fig. 1a) that together discharge 40 % of the ice from West Antarctica to the Ross Ice Shelf (Price et al., 2001). The WIS is one of the fastest-flowing ice streams along the Siple Coast, with velocities greater than  $300 \text{ m a}^{-1}$ , due to its well-lubricated, deformable subglacial bed (Tulaczyk et al., 2000). Negative mass balance (i.e., thinning of the ice column) is observed downstream (Bindschadler et al., 2005; Campbell et al., 2018). However, positive mass balance (i.e., thickening) is present in the upstream region of the WIS. This is because, in the middle of the 19th century, the neighboring Kamb Ice Stream (KIS) stagnated from  $120 \text{ m a}^{-1}$  to a current flow speed of  $10 \text{ m a}^{-1}$  (Retzlaff and Bentley, 1993; Joughin et al., 2002). The stagnated KIS, combined with

thinning of the WIS, has resulted in a diversion of flow from the KIS to the WIS (Price et al., 2001). The result is thickening in the accumulation area of the WIS, estimated at  $1 \text{ m a}^{-1}$  (Bindschadler et al., 1993), which contributes to the deceleration of the WIS at an estimated rate of  $5.5 \text{ m a}^{-2}$  (Beem et al., 2014). The deceleration, combined with bed strengthening that results from frozen ice at the glacier bed, is projected to cause a stoppage of ice flow in the next 40 years (Bougamont et al., 2003).

As a result of the dynamics of fast flow, subglacial hydrology, and basal mechanics, the WIS experiences a wide variety of cryoseismic events. The seismicity ranges from low-frequency ( $10^{-2}$  Hz) basal stick-slip (Winberry et al., 2009b) to possible higher-frequency (10–50 Hz) icequakes (Winberry et al., 2013). Glacier processes on the nearby Ross Ice Shelf exhibit seismicity with frequencies from  $10^{-3}$  Hz ocean gravity waves and swells (Chen et al., 2019) to elastic waves greater than 5 Hz in the near surface from temperature changes (Chaput et al., 2018). These processes from the Ross Ice Shelf could provide indirect seismic sources that can be detected in the external wave field at the WIS (Wiens et al., 2016).

Continuous seismic recordings of the WIS were made between 14 December 2010 and 31 January 2011 inclusive (Winberry et al., 2010). Between the 35 stations deployed, two seismic sensor types were used: the Guralp CMG-40T-1 and Trillium 120 broadband sensors. We use data sampled at 200 Hz from the sites with a Trillium 120 broadband sensor: 17 stations with names of format BBXX (Fig. 1b; triangles). Excluded are stations BB02, BB05, and BB09 due to missing components and/or incomplete data for a significant proportion of the deployment, resulting in 14 seismometers being used for this study.

Cryoseismic events occurring during the 2010–11 instrument deployment on the WIS were identified (Latto et al., 2024) using an implementation of the multi-STA/LTA algorithm (Turner et al., 2021). Two catalogues are produced, a *reference event* catalogue and a *trace* catalogue, which list event information per seismometer. The reference event catalogue (1856 events) summarizes (e.g., averages) event information over the entire seismometer array and therefore summarizes the individual trace catalogue (8696 entries). The reference event arrival time can precede an individual seismometer's detected trace arrival time by half the network time for the three closest seismometers that detect an event. The reference event catalogue therefore maintains the complete duration of an event across the network. Seismic events are preferentially detected across stations (Fig. 1b). For example, station BB07, which is located near to where the highest-power seismic events nucleate during periods of local high tide, detected 1113 events, whereas station BB04, located further from the grounding line and tide-related processes, detected 285 events. The unsupervised learning application described herein makes use of both the reference event and the trace catalogues.

### 3 Unsupervised learning to identify glacier processes

We use an unsupervised learning approach applied to the previously generated catalogue of events (Latto et al., 2024). The machine learning workflow comprises the following steps: (1) construct a dataset of features (temporal, spectral, and polarization attributes of seismic time series) by processing the seismic records, guided by the pre-existing event catalogue; (2) group the events into clusters using the *k*-means++ algorithm according to the similarity between features identified; (3) carry out exploratory data analysis to review and optimize the clusters; (4) identify probable glacier processes from the mechanisms that cause the more consistent clusters through an appraisal of other recorded signals; and (5) interpret the origin of the seismic energy identified in the previous step.

#### 3.1 Constructing a dataset of features

The representation of a seismic event by multiple features exploits all aspects of a waveform by the learning algorithm. We utilize a subset of features applied previously to a landslide seismic record (Provost et al., 2017) and refined for our application to glacier processes (Table S1). We first construct a dataset of features from the waveform data, guided by the metadata in the trace catalogue (included as TraceFeatureDatasetWhillans.csv at [https://github.com/beccalatto/multi\\_sta\\_lta/](https://github.com/beccalatto/multi_sta_lta/), last access: 18 March 2024). Then, we use the trace dataset of features to compute a reference dataset of features that correspond to the reference catalogue (included as ReferenceFeatureDatasetWhillans.csv at [https://github.com/beccalatto/multi\\_sta\\_lta/](https://github.com/beccalatto/multi_sta_lta/), last access: 18 March 2024). Each of the 1856 reference events is thus characterized by a single feature set (as an appropriate average or median) that is representative of the recording stations. For a given event, we compute and sort trace catalogue seismometer records in order from the most energetic (i.e., largest maximum peak amplitude of a record) to the least. For that event, feature values are chosen as the median – or second highest – from the top three most energetic records. Feature-specific computation details are given in Table S1. The feature-specific computations are further described in Part 1 and corresponding software documentation – Latto et al. (2024) and Turner et al. (2021), respectively. From this point onward, when referring to event features we are describing those pertaining to the reference feature dataset.

The set of features for each event is transformed prior to clustering to reduce potential biases. In this context, bias refers to an inconsistent weighting of the importance of a given feature based on numerically large ranges that can unduly influence clustering results because *k*-means relies on geometric (Euclidean) distances (Aksoy and Haralick, 2001; Mohamad and Usman, 2013). First, we review the distribution of each feature to determine a scaling (Table S1). For example, features that quantify energy typically fit exponen-

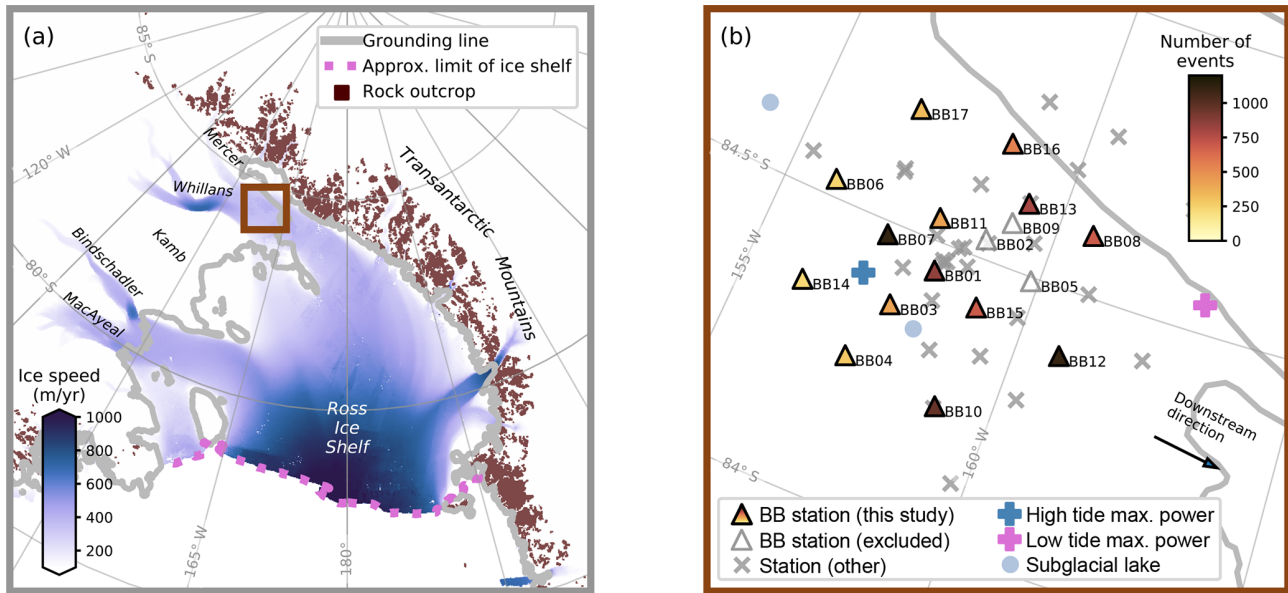


**Figure 1.** WIS dynamics and seismic environment. **(a)** Location of the WIS in the context of the Ross Ice Shelf (BB01: 84°17′43.8066″ S, 158°9′47.1636″ W) with overlaid ice flow speed (Rignot et al., 2011), grounding line (grey line; Rignot et al., 2013; Mouginot et al., 2017), and rock outcrops (Burton-Johnson et al., 2016). **(b)** The WIS temporary broadband stations deployed in austral summer 2010 and 2011. The broadband stations in this study are colored according to the number of events detected per station, retrieved from the trace catalogue of Latto et al. (2024). The blue cross is approximately at the center of the stick-slip region, where the highest-power seismic events nucleate during periods of local high tide (84.4° S, 157° W; Pratt et al., 2014; Barcheck et al., 2018). The pink cross is at approximately the grounding line, where the highest-power stick-slip events nucleate during periods of local low tide (84.55° S, 163° W). The two pale-blue circles indicate subglacial lakes (Wright and Siegert, 2012). Map generated by the “agrid” Python module (Stål and Reading, 2020).

tial distributions and so can be set on a logarithmic scale. Other features that have very narrow ranges (e.g., the rectilinearity range is 1) can incorrectly skew towards values near their minimum when set on a logarithmic scale and so are kept on a linear scale. We carry out a standardization procedure to constrain the features to the same range, centered at zero, by scaling by a feature’s standard deviation. After these transformations, the features retain their diverse distributions but are now on comparable scales, which is important for distance-based clustering algorithms (histograms shown in Fig. 2; box-and-whisker plots shown in Fig. S1).

### 3.1.1 Selection

The next step in our workflow is feature selection, which is applied because the inclusion of too many correlated features in a clustering procedure can yield an artificial weighting. We compute a comparison of each feature pair, quantifying similarity by  $r$ , the Pearson correlation coefficient (Fig. 3). The maximum anti-correlation is  $r = -0.75$ , and the maximum (non-diagonal) correlation is  $r = 0.99$ . We define similar features at  $r \geq 0.95$ , after a careful review of the variance observed in feature relationships below that threshold (e.g., Fig. 3, scatterplot between feature 2 and feature 5 with  $r = -0.75$ ). Within each highly correlated set of features, we choose which feature is most useful to keep for analysis

(scatterplots shown in Fig. S2; reasoning for feature choice provided in Table S2). After removal of a total of 7 features, the input to clustering (our “standard” dataset) contains 30 remaining features to characterize each event.

### 3.2 Grouping the events into clusters

The dataset of selected features is used to find clusters of similar WIS events, by means of the  $k$ -means++ algorithm (Jain, 2010), which employs a standard initialization approach, with the default parameters for improving convergence as defined by the widely used Python implementation (Pedregosa et al., 2011, sklearn.cluster.KMeans). The data matrix used as input to  $k$ -means++ is defined as follows:  $X = x_{ij}$ , where  $i = 1, \dots, m$  and  $j = 1, \dots, N$ , with  $m$  waveforms described by  $N$  features. The algorithm takes the following steps.

1. Initialize  $k$  clusters, where each cluster  $g$  is assigned a seed (centroid)  $\mu_g$  from  $g = 1, \dots, k$ ; i.e., each  $g$  is defined by  $\mu_g = [\mu_{g1}, \mu_{g2}, \dots, \mu_{gj}, \dots, \mu_{gN}]$ .
2. Assign waveforms  $x_{ij}$  to a cluster by minimizing Euclidean distances between all the features of a waveform and a centroid  $\mu$ . The `argmin` function finds the value of  $g$  which minimizes the Euclidean distance. Each waveform  $i$  is assigned to a cluster number  $g$  as

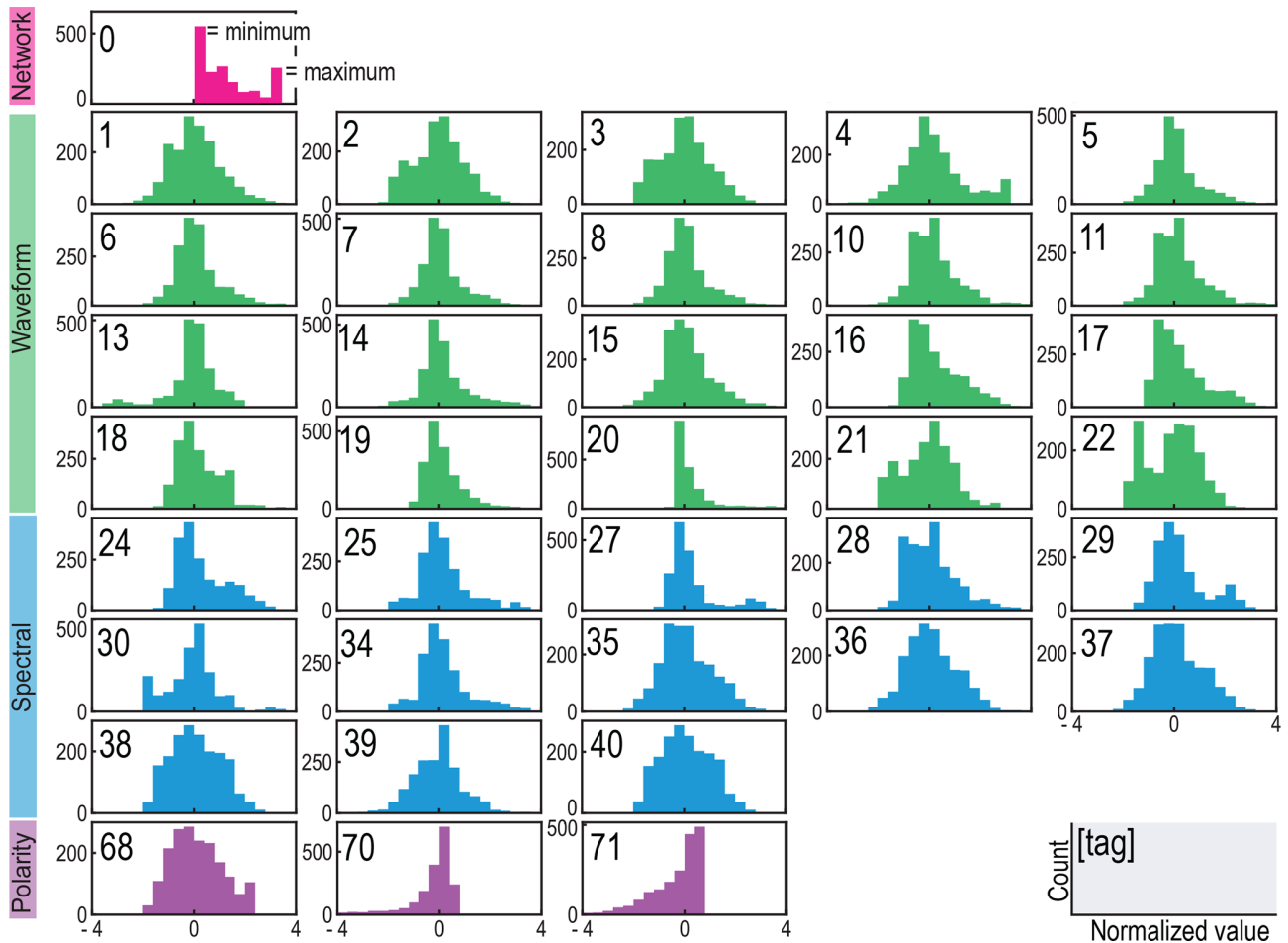


**Figure 2.** Distribution of each feature in the feature dataset after log or linear scaling and standardization. The feature tags (top-left corner of each plot) and color attributions (top to bottom: pink, green, blue, and purple) correspond to the numerical tag per feature and feature types provided in Table S1. Other qualities of each feature, such as the median, minimum, and maximum of each distribution, are provided in a box-and-whisker plot with the same number and color (Fig. S1).

represented by the following expression:

$$c_i = \operatorname{argmin}_g \left( \sum_j^N (x_{ij} - \mu_{gj})^2 \right).$$

3. Recompute the centroid of each cluster based on the mean of the waveform features assigned to each cluster. Each cluster  $g$  is assigned a centroid  $\mu_g$  defined by

$$\mu_{rj} = \frac{\sum_{i=1}^m \delta(c_i, r) x_{ij}}{\sum_{i=1}^m \delta(c_i, r)},$$

where  $\delta$  is the Kronecker delta function.

4. Iterate Steps 2 and 3 until a threshold indicating convergence is reached, i.e., when the centroids are no longer significantly updated.

### 3.3 Exploratory data analysis for optimization

Our implementation of  $k$ -means++ requires the number of clusters ( $k$ ) to be prescribed a priori. Many studies have attempted to appraise the value for  $k$  via statistical techniques (e.g., Legany et al., 2006; Bhargavi and Gowda, 2015). For our application, we show the results of the silhouette test, a widely used estimator that quantifies the tightness of a cluster by computing the Euclidean distance of each  $n$ -dimensional data point to each centroid (Rousseeuw, 1987), in Fig. S3a. This test is, however, less informative when applied to real, noisy data whose clusters are not necessarily well-separated (see Sect. S3.3 for further discussion; Famili et al., 2004; He and Yu, 2019). Therefore, a recommended approach combines user-domain knowledge, which qualifies the usefulness of a clustering result, with statistical metrics, which quantify how well-separated a clustering result is (Zu Eissen and Wißbrock, 2003). We employ a semi-automated methodology that complements the unsupervised  $k$ -means++ algo-

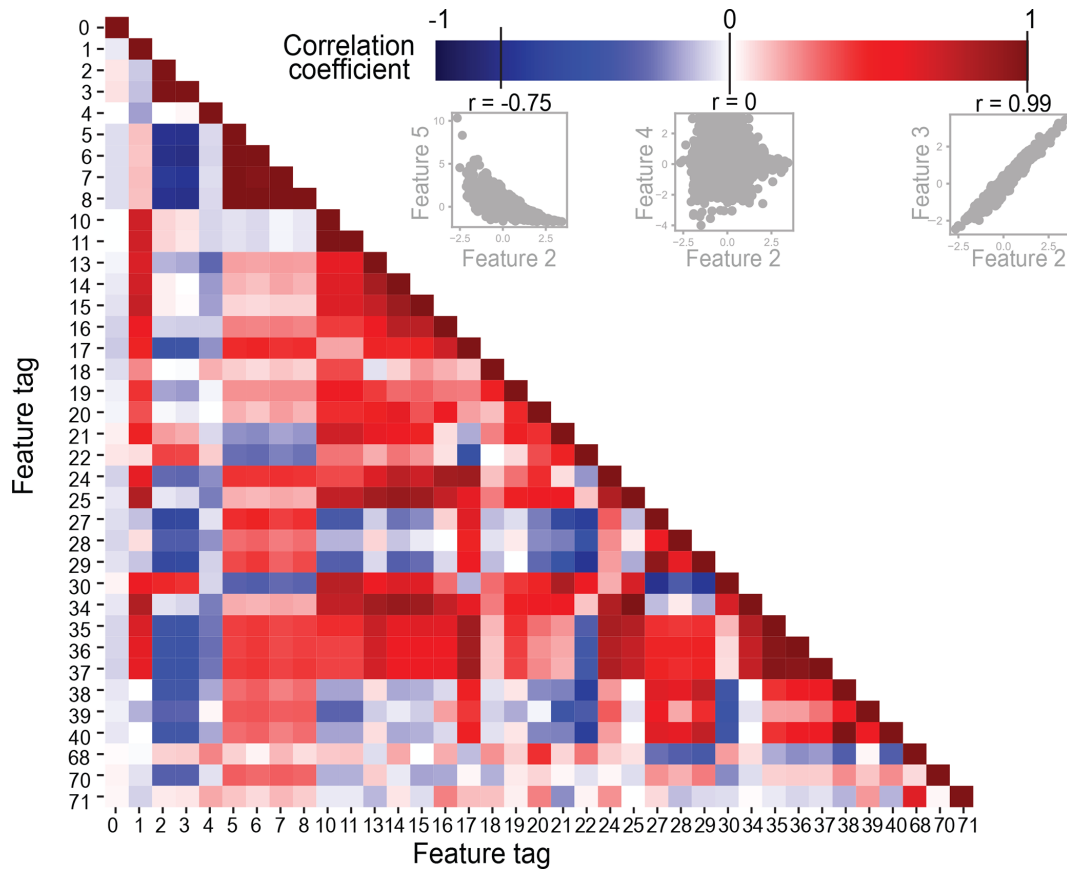


**Figure 3.** Pearson correlation coefficient ( $r$ ) matrix to quantify feature similarity from  $-1$  to  $1$ . The maximum anti-correlation of this dataset ( $r = -0.75$ ) shows that features at this  $r$  value display variance, shown by the scatterplot of an example pair of features, 2 and 5. At  $r = 0$ , there is no correlation, exemplified by another pair of features, 2 and 4. The highest correlation of this dataset is at  $r = 0.99$ , and the strong relationship of features at this correlation coefficient is demonstrated by a third example pair of features, 2 and 3. In this case, feature 2 is removed from analysis. The scatter diagrams of other features with high  $r$  values are provided with details on feature choices (Fig. S2; Table S2).

rithm with an initial manual appraisal of the seismic event database and thorough review of parameter options. We aim to optimize the parameter choice of  $k$  for this application to find clusters of cryoseismic events that can be reasonably matched to known glacier dynamic processes and/or used to investigate new or previously unidentified glacier signals.

### 3.3.1 Evaluating the WIS event catalogue by human analyst

The manual appraisal comprises a thorough search and evaluation of the WIS catalogue by an analyst using a GUI tool designed for this application (Fig. S4). The tool provides fields for recording visually discernible features of an event, such as spectral description and maximum characteristic frequency, emergent behavior, and envelope description. The tool also provides a field to assign each event a probable cluster type, thereby producing an ad hoc labeled dataset of cryoseismic events for the WIS. The labels assigned during the manual search include processes such as “stick-slip” and

“teleseismic” and broader potential attributions to “Other” which is a catch-all category of noise-type events potentially generated from the surrounding Ross Ice Shelf and Ross Sea.

While the manual appraisal is conducted on all events, we have previously assigned low- and high-confidence labels to each event in order to assess relative uncertainty in the dataset (Latto et al., 2024), with 35 % of events being assigned a high-confidence rating. The following cluster analysis and discussion use all events, justified by the low- and high-confidence events presenting with logical patterns in the feature spaces and spatio-temporal domains (see Fig. 4). Figures including “high-confidence events only” are included in the Supplement for a subset of figures (Figs. 4, 5, 6, 7, and 8 with corresponding Figs. S5, S6, S9, S10, and S11).

We verify the manually appraised labels for events where the data are available. First, by comparing the Pratt et al. (2014, Table S4) stick-slip catalogue with the manual-appraisal-labeled stick-slip events, we find 136 of our identified stick-slip events are identified as such by Pratt et al.

(2014) and 4 are newly identified. None of the Pratt et al. (2014) stick-slip events are missed by our method. In this case, by the word “event” we are referring to any segment of stick-slip rupture where the expected WIS stick-slip episode has two to three ruptures in a 30 min span. In later discussions, we refer to the 136 verified stick-slip events as PRA14 (i.e., Pratt et al., 2014) and the 4 additional events as PRA14 additional. The global seismic catalogue (U.S. Geological Survey, 2022) is also used as a cross-reference list with manually appraised teleseisms and other events not necessarily identifiable by eye as teleseisms. We find 68 events are potential teleseisms, which we label in subdivisions as Teleseism I ( $> 3.5 \log$  a.u. peak amplitude, 32 events; a.u. denotes arbitrary units) and Teleseism II ( $\leq 3.5$  peak amplitude, 36 events).

We summarize the results of the manual appraisal for the event catalogue in the bivariate feature relationships of duration, peak amplitude, and characteristic frequency with analyst-appraised labels (Fig. 4). The representation of events in this two-dimensional framework illustrates how clusters are inherently formed by feature relationships. For example, the finding that all events labeled as stick-slip motion have similar durations ( $10^2$ – $10^4$  s), characteristic frequencies ( $10^{-2}$ – $10^{-1}$  Hz), and peak amplitudes ( $10^4$ – $10^5$  a.u.) lends credibility to the potentially mechanistic significance of clustering results. Variations within the features with assigned cluster labels suggest where a different number of clusters and corresponding labels might better suit the feature dataset. Figure S5 (with high-confidence events only) in comparison to Fig. 4 shows that high-confidence events are typically the longer and stronger events. The overall patterns inherent in the clusters, particularly for the stick-slip events, largely remain the same. We highlight that subsequent comparisons of features in the  $k$ -means methodology refer to standardized values where appropriate, which can lead to information loss.

We aim to evaluate the labels assigned to the cryoseismic event types we expect from the WIS using overviews such as Ekström et al. (2003) and Podolskiy and Walter (2016) that document the common feature ranges of cryoseismic events (Table S3). In doing so, we can improve the manual appraisal by, for example, considering distinct labels for some of the broad “Other” events, such as “ocean primary and secondary microseisms”, for durations between 1–10 s and characteristic frequencies of  $10^{-1}$  to 1 Hz.

### 3.3.2 Investigating cluster evolution

By definition, the points in the clusters yielded by  $k$ -means++ with cluster parameter  $k$  will be rearranged when the cluster parameter is increased to  $k+1$  or decreased to  $k-1$ , independently of  $k$ . We are motivated to understand how the seismic events in a cluster split or group as  $k$  changes in order to most reasonably determine the choice of  $k$ , the number of clusters. Typically, studying cluster evolution is challenging due to the

built-in pseudo-randomness of  $k$ -means, which assigns clusters a potentially different nondescript numerical label each time the  $k$ -means problem is solved. Therefore, to more easily identify the clusters as they appear and change for each  $k$  value, rather than rely on the automated  $k$ -means label, we discern clusters by percentage makeups that are recognizable as  $k$  changes, i.e., types of events from manual appraisal in combination with the number of seismic events assigned to each cluster.

We can then apply the  $k$ -means++ algorithm to the standard feature dataset (Sect. 3.1.1) for the number of clusters  $k=2$  (the minimum possible) up to  $k=14$  (a realistic maximum), and evaluate the corresponding solution as it evolves (Fig. 5). The illustration of how clusters merge and split as  $k$  is increased offers two main conclusions. Firstly, as  $k$  increases, typically only one of a set of clusters will split into two clusters, as depicted by the single assigned arrow per row that illustrates where a portion of the seismic events of a cluster will form a separate group. This indicates that if a single cluster appears to represent two distinct types of events, that cluster could be pushed to split when clustering is forced to a solution at  $k+1$ . Secondly, once a larger cluster splits into a new cluster, that new cluster will generally retain its composition as  $k$  increases. For example, the cluster in the second column from the right (i.e., first composed of 7.38 % of the total events) appears to contain approximately the same number and composition of Teleseism I events as  $k$  is increased (Fig. 5). An exception to both findings is shown in the third column from the left (i.e., first composed of 13.63 % of the total events), which is formed by the split part of two clusters, that immediately to the left and the furthest column to the right. This third column cluster splits at  $k=9$ . In routine use of unsupervised learning, detailed investigation of the cluster splits for sequential values of the  $k$ -means++ algorithm would not be expected; however, in this contribution we show cluster evolution to better inform the choice of  $k$ .

In Sect. S3 in the Supplement, we describe the quantitative approaches used to recommend an optimized choice of  $k=10$  (Fig. S3). After contextualizing that choice with the previous appraisal of the catalogue and included discussion on cluster evolution, we choose to proceed with  $k=10$ .

### 3.4 Event clusters and glacier processes

We evaluate the clustering solution for  $k=10$  in order to infer the glacier processes potentially represented for each cluster (Table 1). For ease of reference, the clusters yielded from  $k=10$  are numbered (1–10 in the order shown in Fig. 5). For each cluster, we first make use of the manual appraisal to compute the percentage of events that are attributed to stick-slip processes and teleseismic earthquakes. Cluster 1 and Cluster 2 are assigned the majority of stick-slip events, Cluster 2 is also assigned a minority of Teleseism I events, and Cluster 9 is assigned the majority of Teleseism I and Teleseism II events, all designations that suggest the at-



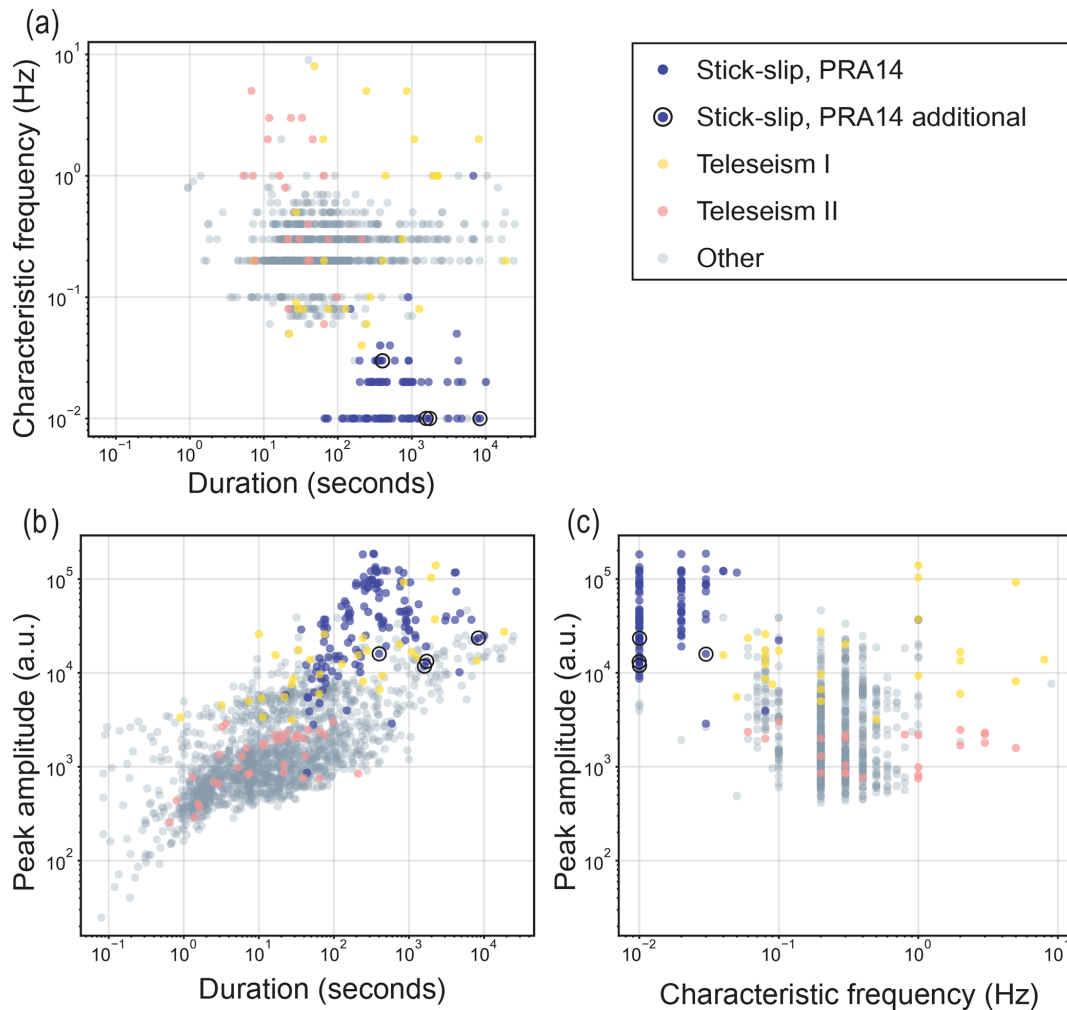


**Figure 4.** Manual appraisal of the reference event catalogue. The features measuring duration (log, seconds) and peak amplitude (log, a.u.) are retrieved from the reference event catalogue, and characteristic frequency (log, Hz) is determined from the spectrograms of each event in the manual appraisal. Event types that are identified from the manual appraisal and further validated in subsequent investigation show the natural groupings, or clusters, of events in each bivariate feature pair: (a) duration and characteristic frequency, (b) duration and peak amplitude, and (c) characteristic frequency and peak amplitude. The manual appraisal of the reference event catalogue showing high-confidence events only is included in Fig. S5.

tributed mechanisms for the clusters. Cluster 2 also contains the four stick-slips indicated as additional to the Pratt et al. (2014) catalogue. Clusters 3, 4, 5, 6, 7, 8, and 10 also contain small (i.e., < 5 %) numbers of teleseismic events. Supporting information regarding the distribution of features per cluster and the features that most differentiate each cluster is provided (Fig. S7).

To further illuminate the underlying physical processes, we analyze the WIS clusters with respect to tidal heights computed at a downstream location (84°20′20.3994″ S, 166°0′0″ W). This shows that Clusters 1 and 2 also vary with regard to occurrence at high and low tides, with Cluster 1 showing a slight tendency towards high tide and Cluster 2 showing a more even split. This result is substantiated by previous studies on distinct modes of stick-slip (stick-slip

variation in event length is dependent on initiation location, i.e., central or near the grounding line, and tide height; Pratt et al., 2014). Cluster 5 events indicate the strongest tidal association with 75.1 % of events occurring at high tides, while Cluster 9 events show a slight tendency towards high tides.

We now explore the spatial and temporal distribution of events that are attributed to clusters (Fig. 6; spatial synthesis in Table S4; temporal synthesis in Fig. S8). From the spatial analysis, we observe that the seismometers detecting the most stick-slip events from Clusters 1 and 2 are located within a previously identified sticky spot (Fig. 6a, called the “central sticky spot”; Winberry et al., 2014; Barcheck et al., 2018) and a lower proportion of events are detected near the grounding line, at seismometers downstream of a subglacial lake (Lake Engelhardt) located at 83.6° S, 159° W (Fig. 6a,

**Table 1.** Characterization of clusters for  $k = 10$  by various measures: the percentage of events that are stick-slip events from the Pratt et al. (2014) catalogue (PRA14) and those additional to the catalogue (PRA14a); the percentage of events that are teleseismic events with amplitudes  $> 3.5$  (log, a.u.; TI) and those with amplitudes  $\leq 3.5$  (log, a.u.; TII); the features that are most discriminant (most positive, +, or most negative, –) and therefore most defining for a given cluster are listed in Table S5; the percent at which a cluster's events occur at high tide (the tidal heights used to gather the percent values are determined for a downstream location ( $84^{\circ}20'20.3994''$  S,  $166^{\circ}0'0''$  W) from the CATS tidal model; Padman et al., 2002; Howard et al., 2019); the four seismometers that detect the majority of events per cluster, in order from most to least (Table S4); the days on which the most events per cluster are detected (Fig. S8 left column); and the hours at which the most events per cluster are detected (Fig. S8 right column).

Cluster	Events, %	Stick-slip events, % (PRA14, PRA14a)	Teleseismic events, % (TI, TII)	Most discriminant features in rank order (+/–)	Positive tidal, %	Spatial	Daily	Hourly
1	7.49	84.2, 0.72	1.44, 0	20 (+), 14 (+), 68 (+), 24 (+), 34 (+), 16 (+)	62.6	BB04, BB14, BB03, BB06	Intermittent	07:00–18:00, 19:00–03:00
2	4.58	15.3, 3.53	8.24, 0	34 (+), 30 (+), 19 (+), 10 (+), 18 (+), 1 (+)	50.6	BB06, BB17, BB11, BB14	Intermittent	00:00, 04:00
3	9.16	1.18, 0	1.18, 1.76	1 (+), 21 (+), 71 (–), 10 (+), 15 (+), 37 (+)	48.2	BB17, BB10, BB08, BB13	7, 15, 18	23:00–05:00
4	6.41	1.68, 0	0, 0.84	4 (+), 19 (+), 20 (+), 22 (+), 10 (+), 21 (+)	54.6	BB15, BB06, BB01, BB07	2–5, 7	00:00–04:00, 14:00–16:00
5	12.3	0, 0	1.75, 0	27 (–), 29 (+), 17 (–), 30 (+), 21 (+), 24 (+)	75.1	BB16, BB15, BB12, BB01	33–34	01:00–12:00, 13:00–16:00
6	9.38	0, 0	0, 3.45	22 (–), 28 (+), 71 (–), 38 (+), 29 (+), 27 (+)	63.8	BB12, BB13, BB07, BB10	5–6, 33–35	09:00–19:00
7	10.6	0, 0	1.53, 2.04	36 (–), 13 (–), 37 (–), 35 (–), 68 (+), 3 (+)	56.1	BB13, BB01, BB07, BB10	Intermittent	00:00–05:00, 12:00–17:00
8	5.71	0, 0	0, 3.77	13 (–), 4 (+), 36 (–), 35 (–), 14 (–), 34 (–)	68.9	BB12, BB13, BB07, BB10	Intermittent	01:00–05:00, 11:00–16:00
9	7.17	0, 0	10.5, 5.26	70 (–), 16 (+), 3 (+), 14 (+), 38 (–), 5 (–)	64.7	BB04, BB17, BB03, BB11	7, 11, 19, 30, 35	13:00–22:00
10	27.2	0.40, 0	0, 2.18	71 (–), 39 (–), 17 (–), 37 (–), 16 (–), 35 (–)	59.0	BB13, BB08, BB07, BB12	Intermittent	00:00–04:00, 14:00–16:00

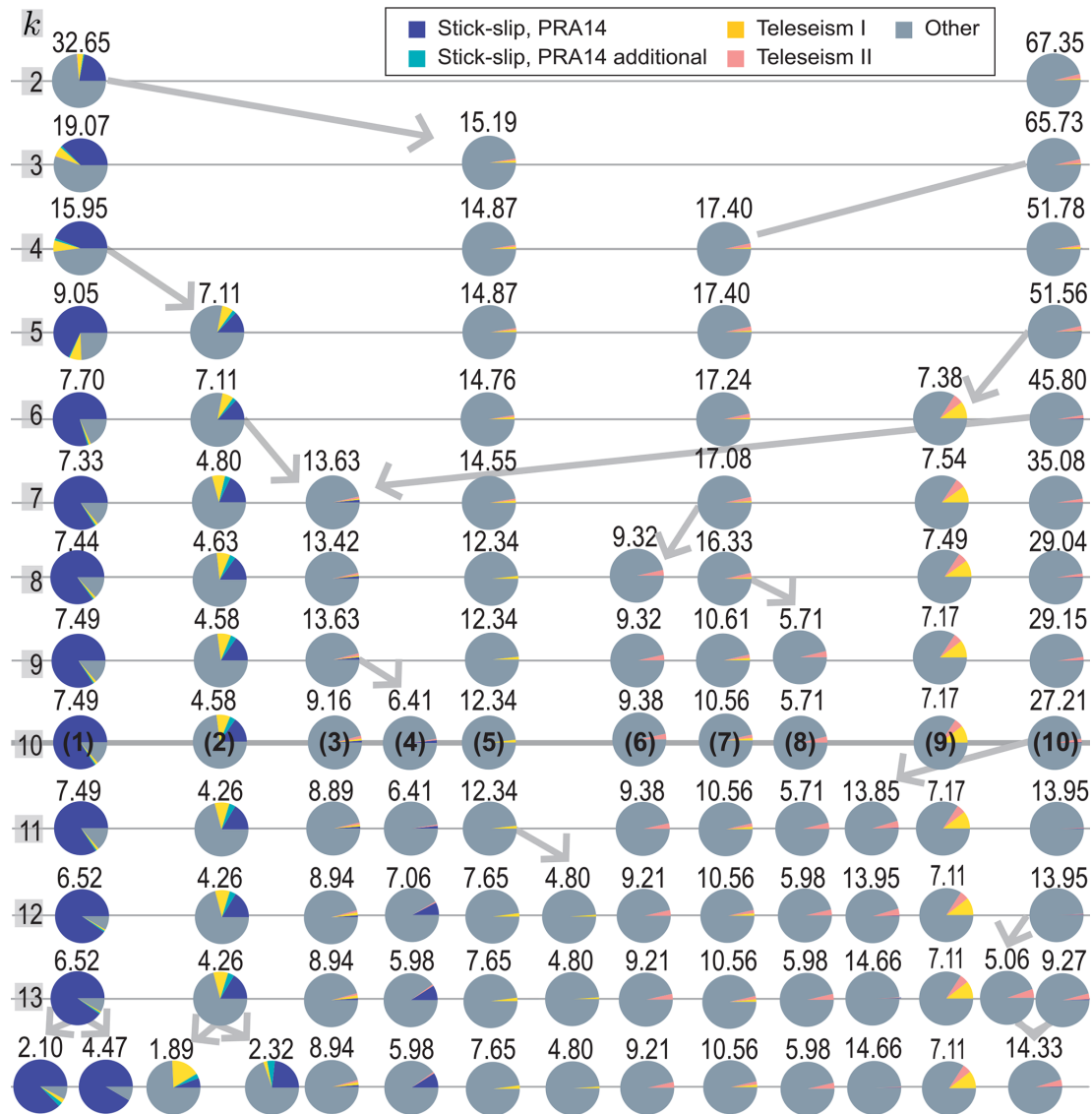


**Figure 5.** Illustration of how clusters (depicted as circles) evolve in composition from  $k = 2$  (top row) to  $k = 14$  (bottom row). As  $k$  increases (top to bottom), each column tracks an individual cluster and arrows indicate when a cluster splits or merges. The heavy grey line at  $k = 10$  indicates the preferred value of  $k$ ; along this row, cluster numbers are counted from left to right (1 to 10) and match those in Table 1 and Figs. 6 and 7. The number above each cluster is the percentage of total events; thereby the numbers across a row sum to 100 %. Pie chart segments represent the percentage of events within a cluster, as labeled with an event type during the manual appraisal. Clusters 3, 4, 6, 7, 8, and 10 contain events best characterized as noise types based on the majority labeled as “Other” and their features (Sect. 3). Clusters 1, 2, 5, and 9 contain labeled events and/or noise that appears related to processes by further analysis. Event types as identified by manual appraisal are shown in the legend; further event types identified by unsupervised learning (Fig. 6) occur in Cluster 5 (events from an icequake swarm, lasting 2 d). An illustration of how clusters evolve in composition from  $k = 2$  to  $k = 14$  showing high-confidence events only is included in Fig. S6.

Pratt et al., 2014). The temporal analysis highlights a unique type of event occurring on 16 January and 17 January 2011, as all of Cluster 5 can be traced to these dates (Fig. 6b). Cluster 9 containing teleseismic events (about 16 %) also contains events manually appraised as “Other” that have similar high-energy signatures to the high-amplitude teleseisms (Fig. S7). In the spatio-temporal attribution, we find that these events

appear grouped in the time interval between 14 and 21 h after 00:00 UTC. Preceding solar noon (22:00 to 23:00 UTC), this diurnal pattern could indicate a partial control due to changes in surface ice temperature (Fig. 6b).

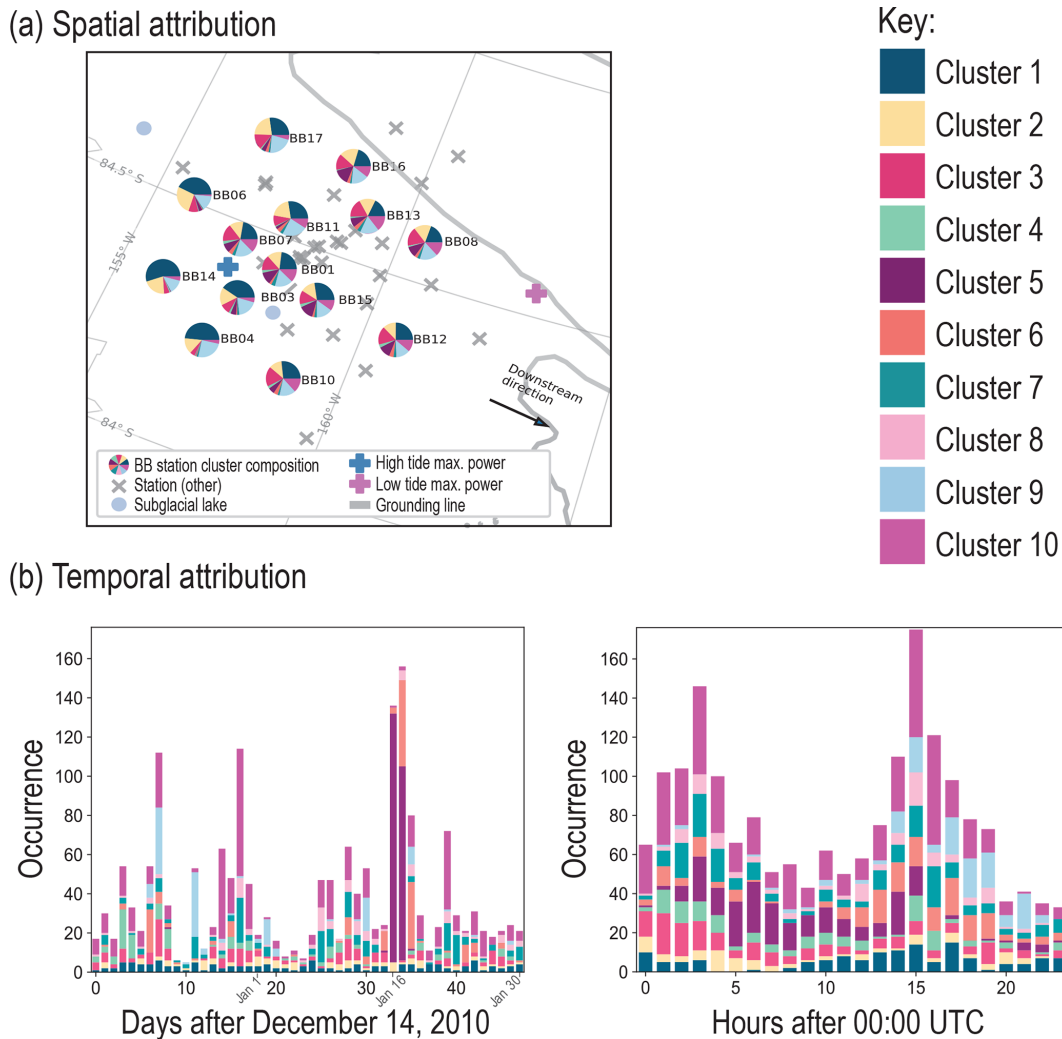


**Figure 6.** The (a) spatial and (b) temporal attribution of clusters for  $k = 10$ . The spatial attribution pie chart segment colors correspond to the numerical cluster assignments provided in the key. The temporal attribution is provided as a daily occurrence for days after 14 December 2010, with annotated reference dates 1, 16, and 30 January and an hourly occurrence for hours after 00:00 UTC, where solar noon falls in the time zone of 22:00 UTC. In conjunction, both attributions are used to better characterize the clusters for  $k = 10$ . The results of the spatio-temporal analysis are synthesized in Table 1. A breakdown for the spatial attribution and temporal attribution is provided in the Supplement (Table S4 and Fig. S8, respectively). Colors were chosen for clarity between separate classes (Glynn and Naylor, 2021, Ordnance Survey). A spatial and temporal attribution of clusters for  $k = 10$  showing high-confidence events only is included in Fig. S9.

## 4 Limitations and discussion

We have demonstrated a step-by-step methodology for applying cluster analysis to a catalogue of seismic events recorded on a soft-bedded Antarctic ice stream. In this section we describe the limitations of this analysis with a view to informing further studies. We then outline the improved understanding of dynamic and hydrological processes at the WIS and in the surrounding region that this study has enabled together with the wider applicability of the methods and workflows.

### 4.1 Algorithm limitations

The choice of  $k$ -means++ was made based on the requirement to use a simple and transparent approach such that the clustering of events and event-like noise as an aid to event catalogue reconnaissance could be investigated and understood. While the results of the event clustering are apparently robust and yield useful insights (discussed below), we here outline some of the potential shortcomings of this algorithm choice and note other options that could be considered in future studies.

Care should be taken when using  $k$ -means, which seeks to optimize similarity (i.e., minimize distances) within each

cluster and favors a smaller parameter space; as the number of features increase, similarity can become a less meaningful metric because of the greater likelihood of overlapping clusters (i.e., “curse of dimensionality”). However, more features introduce potentially useful information into the clustering algorithm. We consider methods of dimensionality reduction for  $k$ -means in Sect. 4.2. We also recognize that while the clusters identified in this study are reasonably robust, they are not especially well separated, and other algorithms could be considered instead. Though beyond the scope and purpose of this paper, the Gaussian mixture model could be investigated in future research as a soft clustering alternative to  $k$ -means.

#### 4.2 Feature transformation: representation, extraction, and selection

Transformation of raw data into a feature set prior to clustering needs to balance preserving information with reducing dimensions. In our application, the first step in this process is feature normalization, in which the raw data fields are each standardized by converting them into the same range of values using standard deviation. This step is considered essential for most clustering algorithms to remove potential biases (Mohamad and Usman, 2013; Trebuña et al., 2014). However, the homogenization of a feature set can also sacrifice information that a clustering algorithm could use to improve the separation of clusters. Other feature representations can be considered in future studies, such as a non-normalized feature set or a feature set standardized by a different approach that retains more information (e.g., quantile transformations).

As a next step in our application, feature selection, or the elimination of highly correlated and/or inconsequential features prior to clustering, is an important step to reduce input bias and dimensions. In a supervised learning application, such as Provost et al. (2017), feature selection can be guided by the quantified error in clustering output based on a labeled, expected result (Breiman, 2001). In the current study, we carried out an evaluation to determine which features are most discriminant using a correlation analysis (Sect. 3.1.1). Further, it can be informative to examine how the clusters change if shown a similar, alternative feature set.

We compare the stability of the clusters that result with  $k = 10$  by clustering events using (a) our standard feature set, (b) all of the features from Table S1 (no selection and elimination), and (c) a halved feature set (Fig. 7). This result shows that the no-elimination option results in about half of the clusters becoming less defined in comparison to the standard feature set. The halved feature set comprises 17 of the less correlated feature pairs from Fig. 3; i.e., a maximum number of features are eliminated, in comparison to the standard set where a minimum number (i.e., only the most correlated) are eliminated. The percent composition of events in the halved set is comparable to the standard, but again, some redistribution of events occurs, significantly impacting about

half the clusters. The distribution in clusters of the positively identified glacier processes remains stable in the halved feature set, so it appears to be more useful to eliminate too many features rather than too few.

We also evaluate the stability shown in Fig. 7 with the high-confidence events only (Fig. S10). This result is used as an additional way to discuss the robustness of each cluster. We find that Clusters 1, 2, 3, 5, 6, and 9 all appear well-defined (i.e., more robust) across the other feature set scenarios. The other clusters (4, 7, 8, and 10) indicate higher instabilities (i.e., less robust) in how the contained events are partitioned. Such a result provides insight into other dimensions of similarity across the noise-type events that conflict with the current feature domain boundaries.

An alternative approach to reducing the number of features that could be considered in other studies is to reduce the dimensionality of the feature space. A common and simplistic approach to dimensionality reduction is principal component analysis, which transforms high-dimensional data into fewer dimensions (called the principal components) by linear decomposition (Hotelling, 1933). Some competitive methods that instead apply nonlinear mapping can often better retain the structure of features in fewer dimensions and include curvilinear component analysis (Demartines and Héroult, 1997), t-SNE (Van der Maaten and Hinton, 2008), and UMAP (McInnes et al., 2018). Other studies would need to investigate the advantages of dimensionality reduction methods as applied to seismic features for clustering analysis.

#### 4.3 Cluster number and assignment of process

The choice of the number of clusters is understood as a significant challenge in the application of  $k$ -means++ because it is difficult to fix a number that captures all the levels of variability in a dataset (Hardy, 1996). While many studies have explored a plethora of approaches, ultimately, the decision requires knowledge of the user domain and is therefore problem-dependent (Jain and Dubes, 1988). We recommend that future studies make use of the methodology, assessing how clusters split or remain stable (Sect. 3.3) to best understand the groups of events represented in each cluster. Such a framework provides a way to ascertain that clusters, or parts thereof, capture distinguishable, physical mechanisms of ice stream dynamics and hydrological processes.

The semi-automated approach combines the power of unsupervised learning with information from prior or independent manual analysis to inform the interpretation of clusters. For example, the tidal influence on stick-slip events is a previously identified relationship between seismicity and temporal cycles (Winberry et al., 2014), and this study extends that understanding. We infer that these events exhibit two different characteristic lengths and occur at the central sticky spot and the grounding line (Fig. 6). This thus enables us

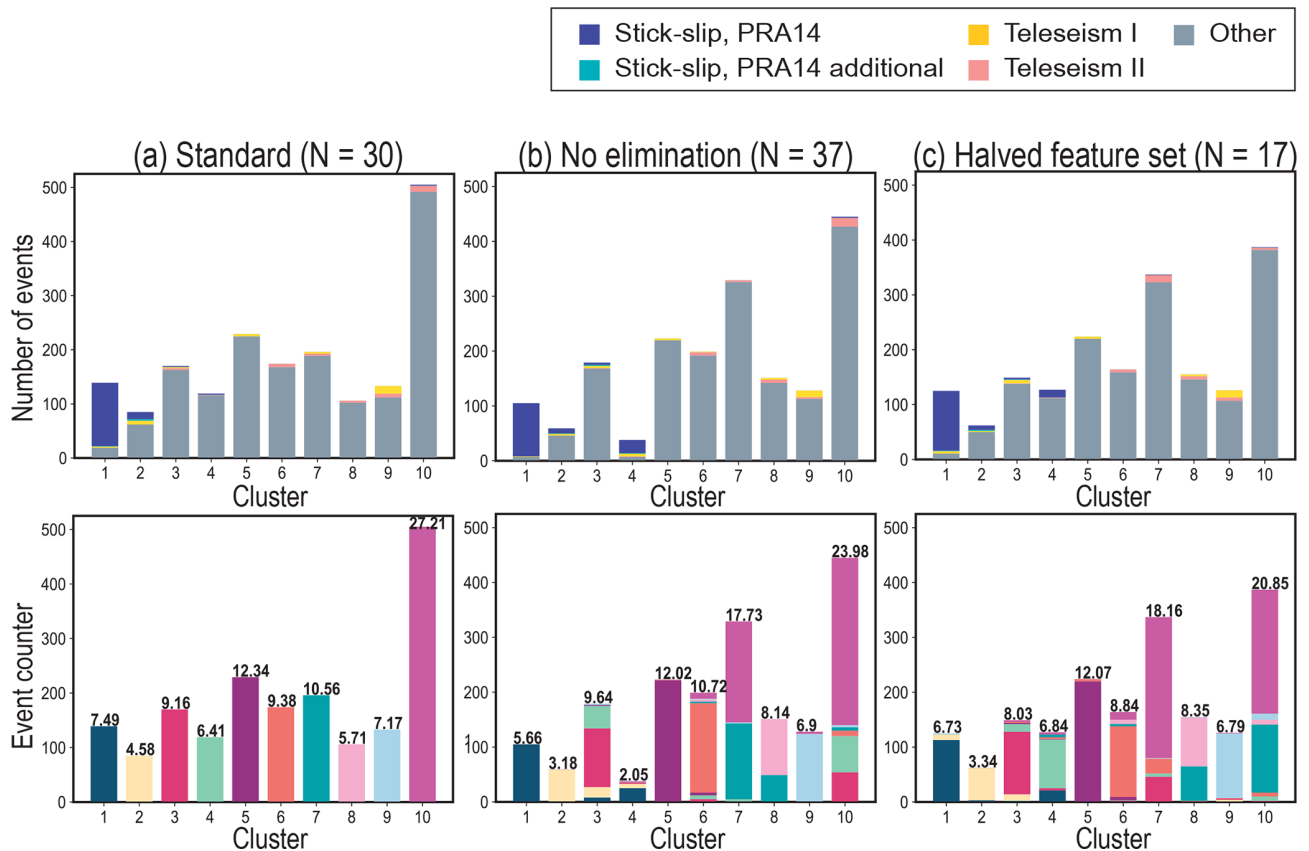


**Figure 7.** Stability of cluster results compared with the standard procedure. From columns left to right, we show (a) the standard set of features after removal of selected members of the feature pairs with  $r \geq 0.95$ , (b) the results of clustering with no features eliminated, and (c) the results with a halved feature set. The top row shows the percentage composition of each cluster, Clusters 1–10, as determined from the manual appraisal. The bottom row provides the number and percentage of events that are grouped in each cluster. The order and labeling of the clusters in the (b) and (c) columns are manually decided by a comparative method that matches clusters approximately 1-to-1 for each application, when possible, noting as a caveat to comparison the pseudo-randomness of  $k$ -means. The colors within each cluster in the bottom row signify where the contents of the clusters resulting from applying the algorithm to the standard feature are placed in the two comparison applications of the algorithm. The stability of cluster results compared with the standard procedure showing high-confidence events only is included in Fig. S10.

to investigate how the spatio-temporal association of these events can relate to tidal influences.

The heuristic technique that we have used in this study has enabled the pre-existing understanding of glacier processes active on the WIS to be extended and has also newly enabled the discovery of other active processes in the WIS dataset that match mechanisms reported elsewhere. These results confirm the value of using an unsupervised learning approach.

#### 4.4 Identified glacier processes and other signals

In our demonstration study, 136 stick-slip events were identified previously in the WIS dataset (Pratt et al., 2014) and 4 have been found in addition by the event detection and semi-supervised learning workflow. High-energy stick-slip events that are mainly initiated from the central sticky spot during high tide, on a diurnal cycle, are contained in Clus-

ter 1 (Fig. 5). A lower proportion of these events are initiated closer to the grounding line and occur during low tide. The Cluster 1 events correspond to both first and the second ruptures of stick-slip, a result consistent with the initiation locations expected for first ruptures (central sticky spot or grounding line depending on high and low tides, respectively) and second ruptures (near grounding line). Stick-slip events contained in Cluster 2 are of higher energies and mostly span both the first and second ruptures (i.e., are longer in total duration). These events are associated with both high and low tides and are detected evenly across the central sticky spot and grounding line, likely because of the even influence of tidal control. The Cluster 2 type of stick-slip events is grouped in the same cluster as comparatively long and energetic telesseismic events (of type Telesseism I).

Further newly identified events occur in the hours preceding solar noon with an irregular periodicity of 4–11 d. These

high-energy events (detected as low strength) propagate horizontally from the far field and group with events (16 %) manually identified as teleseismic events in Cluster 9 (Fig. 5). From the feature-based analysis, we suggest that these signals could be generated externally to the WIS, potentially from the Ross Ice Shelf. Although the signals that we observe have longer frequencies, the mechanism could be related to contraction due to cooling or to cracking triggered by stress from local melt (Hudson et al., 2020). The Cluster 9 non-seismic events therefore suggest mixed diurnal influences (MacAyeal et al., 2019).

We detected a swarm of low-energy, high-frequency events that are unique to 2 d of the deployment: 16 and 17 January 2011. This event swarm is contained in Cluster 5 (Fig. 5) and shows a spatial pattern consistent with the events occurring near the grounding line (Fig. 6) and a temporal pattern linked to high tide (75.1 % occurring at a positive tidal anomaly; Table 1). The lower energies of these events and the relative high frequencies (Fig. S7; Table S5) could indicate that these events originated externally to the WIS, and so the energy was relatively attenuated by the time of arrival (Pérez-Campos et al., 2003). The association with the grounding line and tidal cycles could indicate that these events originated on the Ross Ice Shelf, where tidally induced seismicity has recently been recorded near the ice shelf grounding line (Cole, 2020) and high-frequency ambient resonance during a several-day period can be caused by a surface melt event (Chaput et al., 2018; Jenkins et al., 2021). Process swarms of this nature require a detection mechanism with a high temporal resolution and show the advantage of using seismic methods as part of the toolbox for understanding glacier processes.

A minority of detected events are related to the dynamic glacier processes; the rest are related to the noise field external to the glacier (Fig. 5). The diversity in the noise events is of significant interest as this informs the understanding of cryoseismic and ambient seismic processes in the wider Ross Ice Shelf region. Understanding the diversity of signals is also of utility in understanding the output of the multi-STA/LTA algorithm (used to generate the underlying event catalogue) in terms of identifying events as local to the ice stream or external to the ice stream. Events characterized by long durations, high energies, and tremor-like behavior that occur mainly on several days at the beginning of the deployment period in December 2010 make up Cluster 3. Cluster 4 events have similar temporal structure and high energies but slower emergence, preceding the tremor-like behavior, and overall shorter durations. Short, energetic signals that appear mostly between 16–18 January, concurrent with the Cluster 5 icequake swarm, are represented in Cluster 6. Noise-type events that have similar spatio-temporal occurrences are grouped into Clusters 7 and 8, with the lower-energy events contained in Cluster 8. Cluster 10 contains events with low energies across all frequency bands, spatial associations with the grounding line, and diurnal patterns intermittently

through the deployment. Collectively, the noise-type ambient signals in these clusters, likely related to processes from the nearby Ross Ice Shelf and Ross Sea, are heterogeneous but cluster in a range of frequencies ( $10^{-1}$  to 1 Hz, Fig. 4). This result is useful for guiding future monitoring applications.

As a final comparative summary, the domain of each cluster in the duration–frequency space is shown in Fig. 8 as a snapshot of the Whillans Ice Stream seismicity, in terms of labeled event types (e.g., stick-slip and teleseism) and the other process- and noise-related events made possible by unsupervised learning. An overview of each cluster, its most likely source mechanism, and other comments are provided in the Supplement (Table S6). The manual appraisal has provided a foundation for identifying further event types and their domain boundaries in duration–frequency space. Figure S11, showing high-confidence events only of Fig. 8, offers further insight into the groupings of duration–frequency domains. For example, high-confidence Cluster 9 events not labeled as teleseisms primarily occupy an intermediary duration–frequency domain of 20–120 s and 0.5–0.1 Hz.

#### 4.5 Applicability of approaches

The workflow presented enables a cryoseismic event catalogue, previously built using a straightforward, systematic detection algorithm (Latto et al., 2024), to be analyzed using a similarly transparent approach to a data-driven investigation, i.e., using *k*-means++ and analysis of clusters. While the workflow has been demonstrated for the Whillans Ice Stream, this is a widely applicable approach, which could be used as a benchmark procedure for glacier investigations and monitoring and many other environmental seismology applications. The procedure is well-suited to cases where the recorded seismicity consists of varied event types in a similarly varied ambient wave field. The workflow requires a manual appraisal of events, resulting in plots (Fig. 4) that show an overview of the event populations that are present and reveal useful domains of the feature space. This information is used, as has been demonstrated (Fig. 5; Table 1), in tandem with the unsupervised clustering to understand how the events due to glacier processes are held within the automatically identified clusters.

As one application of the method, comparisons could be made for one glacier from year to year, making use of the very fine temporal resolution and ability to detect hidden processes that comprise the advantage of cryoseismic approaches. After the semi-automated reconnaissance of the first year (manual and unsupervised approaches being used together), this work can be used in subsequent years to streamline unsupervised learning with a greater proportion of automation. Thus it would be possible to undertake a sequence of studies in time, year after year, to detect changes in the spatial and temporal distribution of known processes and to identify new, potentially hidden processes.

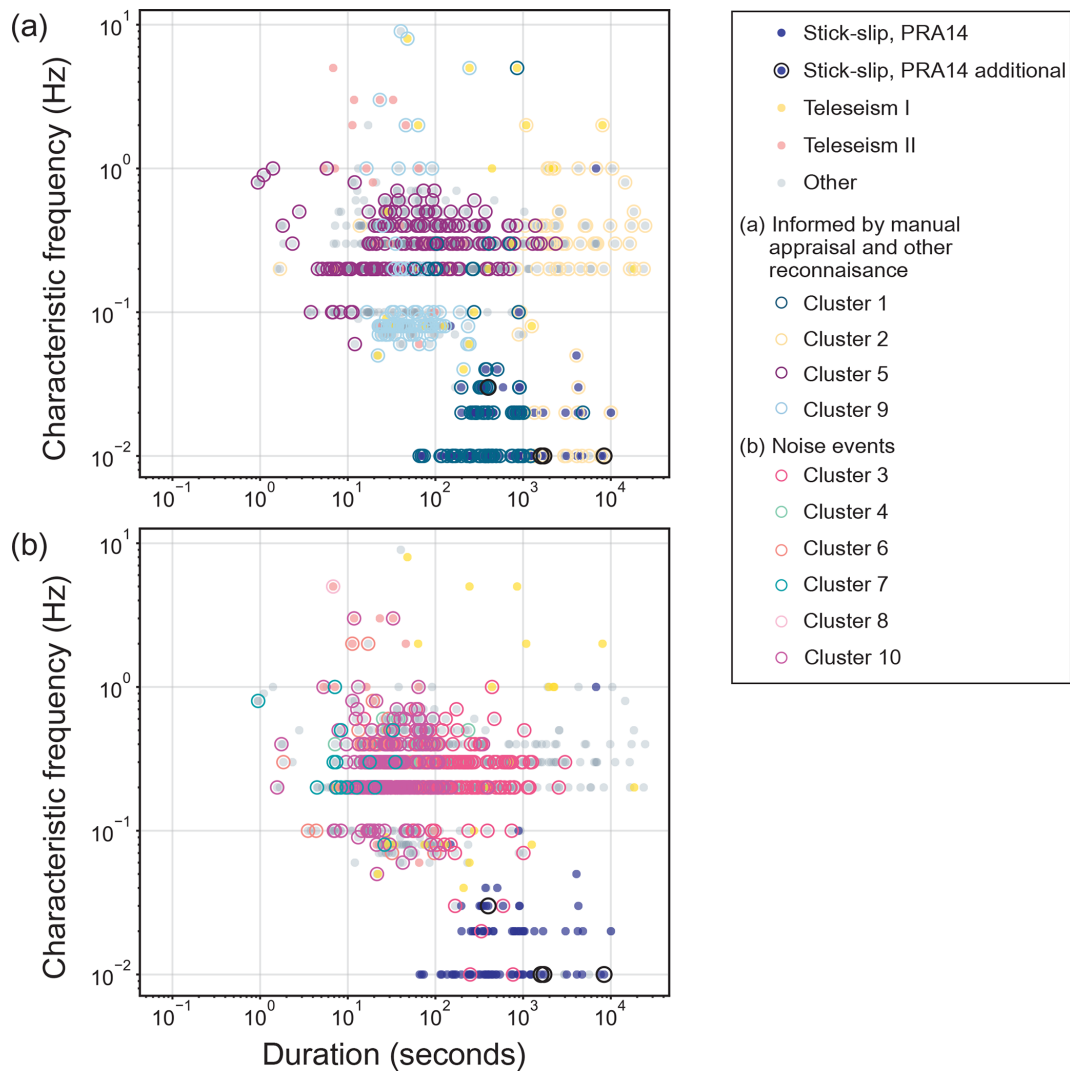


**Figure 8.** Synthesis of the Whillans Ice Stream duration and frequency relationships by manually identified event types and unsupervised learning clusters. The manually identified events are designated by filled circles. The clusters are shown in the two plots as (a) clusters informed by manual appraisal and other reconnaissance, including Cluster 1 (stick-slip), Cluster 2 (stick-slip), Cluster 5 (potentially melt pulse swarm), and Cluster 9 (teleseismic and potentially external fracture-related), and (b) clusters likely pertaining to noise-type events, including Clusters 3, 4, 6, 7, and 8. Some event types can be concealed by other symbols; the events of type “Other” and other manually identified events are arranged in the background such that the unsupervised learning result is in the foreground. A synthesis of the Whillans Ice Stream duration and frequency relationships in Fig. S11 shows only high-confidence events.

The standardization of the method also enables robust comparisons between locations, with bivariate feature plots (Fig. 4) forming a basis for such investigations. Comparative analyses could inform the similarities and differences between event populations in each location and could be further developed using the framework for semi-automated analysis used herein. The clustering of events recorded on the WIS, including event mechanisms that are local to the glacier and also those that are part of the surrounding seismic ambient noise wave field, could be used as a guide to what might be expected at other localities and/or from other deployments.

## 5 Conclusions

Motivated by the potential for data-driven approaches to characterize the diverse signals recorded from glacier environments on the margins of ice sheets, including both local events and ambient noise signals, we have presented a workflow that makes use of semi-automated learning. As a demonstration example, we have shown how glacier processes may be investigated using seismic events recorded on the Whillans Ice Stream. We use a near-comprehensive event catalogue of the 2010–2011 austral summer (Part 1, Latto et al., 2024), from which we form a dataset that represents



each event by a selected set of 30 seismic time series features (attributes). Application of an unsupervised learning algorithm, *k*-means++, to the feature dataset produced 10 best-separated clusters (groups with similar characteristics) of seismic events. These were analyzed with the benefit of a manual appraisal of the catalogue. Although the clusters are only moderately separated, they nevertheless enable valuable reconnaissance analysis.

We identified the following glacier processes: high-energy stick-slip events that are mainly initiated from the central sticky spot, longer and higher-energy stick-slip events initiating near both the central sticky spot and the grounding line, high-energy events that propagate horizontally from the far field generated as part of the external wave field with a diurnal pattern. The latter group of signals could be caused by processes on the Ross Ice Shelf such as contraction due to cooling or to cracking triggered by stress from local melt. We found a swarm of high-frequency events that are unique to 2 d of the deployment: 16 and 17 January 2011, and suggest a relationship to a Ross Ice Shelf melt pulse. The moderate tidal control on the overall event catalogue is seen in the stick-slip events (as previously identified by Pratt et al., 2014) and also the swarm pattern and is also evident to some extent throughout the large number of noise-like events in the catalogue (Latto et al., 2024).

The majority of detected cryoseismic processes are likely related to the complex noise field external to the glacier. By means of clustering, a reconnaissance analysis is enabled, showing signals with a diversity of durations, energies, and behavior (e.g., tremor-like). The variability we find in the ambient noise illustrates an additional challenge for cryoseismic analysis. It is necessary to separate the multiple different local glacier processes listed above from the diverse signals and changing amplitude levels of the seismic ambient wave field. For the Whillans Ice Stream, noise signals cluster within a range of frequencies separated from the domain occupied by some of the process-related events, between  $10^{-1}$  and 1 Hz. Clustering approaches will enable automated methods to be used with a much smaller component of human analyst review in future monitoring of the Whillans Ice Stream using seismic methods.

The demonstration workflow enables a transparent approach to data-driven investigation of glacier processes with seismic signals. The potential for applying unsupervised learning algorithms to cryoseismic signals is vastly improved by a methodical assessment of cluster attribution. That is, future investigations can take better advantage of unsupervised learning methods, following such an initial semi-automated appraisal that includes a manual component, so the semi-automated methodology can continue to identify new event types on a glacier from year to year. An extended investigation into the diversity of local events and ambient noise from a given glacier seismic deployment would enable glacier monitoring, using seismology, for that key location. Future investigations could take advantage of the new methods

and workflows that we have presented, which should prove widely applicable to identifying changes in glacier environments and comparing locations as they respond to the changing global climate.

*Code and data availability.* The trace and reference seismic event catalogues (Sect. 2) and the trace and reference feature datasets (Sect. 3.1) are made available via <https://doi.org/10.5281/zenodo.11062069> (Latto, 2024). Both are produced by extensions to ObsPy software made available (<https://doi.org/10.5281/zenodo.5499909> (Turner et al., 2021)). The results of the *k*-means analysis (Sect. 3.2) are also provided in [https://github.com/beccalatto/multi\\_sta\\_lta/](https://github.com/beccalatto/multi_sta_lta/) (last access: 18 March 2024) by a merged reference catalogue with selected features and cluster labels. Related data for analysis are publicly available: the Whillans Ice Stream seismic dataset is accessible from The IRIS Data Management Center (IRIS-DMC) (<http://ds.iris.edu/mda/2C/?starttime=2010-01-01T00:00&endtime=2011-12-31T23:59:59>, last access: 18 March 2024) ([https://doi.org/10.7914/SN/2C\\_2010](https://doi.org/10.7914/SN/2C_2010); Winberry et al., 2010). The Tide Model Driver (TMD) toolbox ([https://github.com/EarthAndSpaceResearch/TMD\\_Matlab\\_Toolbox\\_v2.5](https://github.com/EarthAndSpaceResearch/TMD_Matlab_Toolbox_v2.5), Erofeeva et al., 2020) allowed for appropriate use of the Circum-Antarctic Tidal Simulation (CATS) (<https://www.esr.org/research/polar-tide-models/list-of-polar-tide-models/cats2008/>, last access: 18 March 2024, and <https://doi.org/10.15784/601235>, Padman et al., 2002; Howard et al., 2019) to compute tidal heights at the Whillans Ice Stream.

*Supplement.* The supplement related to this article is available online at: <https://doi.org/10.5194/tc-18-2081-2024-supplement>.

*Author contributions.* RBL developed software, carried out data analysis, and wrote the text; RJT developed software and provided guidance; AMR gave overall project direction and provided guidance; SC, BK, and JPW advised on the dataset and provided background context. All authors contributed to the refinement of the text.

*Competing interests.* The contact author has declared that none of the authors has any competing interests.

*Disclaimer.* Publisher's note: Copernicus Publications remains neutral with regard to jurisdictional claims made in the text, published maps, institutional affiliations, or any other geographical representation in this paper. While Copernicus Publications makes every effort to include appropriate place names, the final responsibility lies with the authors.

*Acknowledgements.* This research was funded under Australian Research Council Discovery Project DP210100834, with additional support from DP190100418 and ARC's Special Research Initiatives: the Australian Centre for Excellence in Antarctic Science,

SR200100008, and the Australian Antarctic Program Partnership. In addition to the newly available code as above, we used software from the ObsPy Python project (Beyreuther et al., 2010; Megies et al., 2011; Krischer et al., 2015), Fig. 1 was generated by the agrid Python module (Stål and Reading, 2020) with assistance from Tobias Stål. We also wish to thank our colleagues Tobias Stål, Hannes Hollmann, Ian Kelly, and other UTAS–IMAS group members and collaborators for contribution to discussions. We thank the two anonymous examiners of the master of science thesis (for Rebecca Latto, Author 1) in which this research has been included as a core chapter for their careful review of the material and thoughtful suggestions for improvement.

*Financial support.* This research has been supported by the Australian Research Council (projects DP210100834, DP190100418) with additional support from ARC's Special Research Initiatives (Antarctic Gateway Partnership, SR140300001; Australian Centre for Excellence in Antarctic Science, SR200100008).

*Review statement.* This paper was edited by Evgeny A. Podolskiy and reviewed by Clement Hibert and one anonymous referee.

## References

- Aggarwal, C. C., Hinneburg, A., and Keim, D. A.: On the surprising behavior of distance metrics in high dimensional space, in: Database Theory – ICDT 2001: 8th International Conference London, UK, 4–6 January 2001, Proceedings 8, 420–434, Springer, 2001.
- Aksoy, S. and Haralick, R. M.: Feature normalization and likelihood-based similarity measures for image retrieval, *Pattern Recogn. Lett.*, 22, 563–582, 2001.
- Anderberg, M. R.: Cluster analysis for applications: probability and mathematical statistics: a series of monographs and textbooks, vol. 19, Academic press, 2014.
- Arthur, D. and Vassilvitskii, S.: k-means++: The advantages of careful seeding, *Tech. rep.*, Stanford, 2006.
- Aster, R. and Winberry, J.: Glacial seismology, *Reports on Progress in Physics*, 80, 126801, <https://doi.org/10.1088/1361-6633/aa8473>, 2017.
- Barcheck, C. G., Tulaczyk, S., Schwartz, S. Y., Walter, J. I., and Winberry, J. P.: Implications of basal micro-earthquakes and tremor for ice stream mechanics: Stick-slip basal sliding and till erosion, *Earth Planet. Sc. Lett.*, 486, 54–60, 2018.
- Beem, L., Tulaczyk, S., King, M., Bougamont, M., Fricker, H., and Christoffersen, P.: Variable deceleration of Whillans Ice Stream, West Antarctica, *J. Geophys. Res.-Earth Surf.*, 119, 212–224, 2014.
- Benn, D., Gulley, J., Luckman, A., Adamek, A., and Glowacki, P. S.: Englacial drainage systems formed by hydrologically driven crevasse propagation, *J. Glaciol.*, 55, 513–523, 2009.
- Bergen, K. J. and Beroza, G. C.: Earthquake fingerprints: Extracting waveform features for similarity-based earthquake detection, *Pure Appl. Geophys.*, 176, 1037–1059, 2019.
- Bergen, K. J., Chen, T., and Li, Z.: Preface to the focus section on machine learning in seismology, *Seismol. Res. Lett.*, 90, 477–480, 2019.
- Beyer, K., Goldstein, J., Ramakrishnan, R., and Shaft, U.: When is “nearest neighbor” meaningful?, in: Database Theory – ICDT'99: 7th International Conference Jerusalem, Israel, 10–12 January 1999, Proceedings 7, 217–235, Springer, 1999.
- Beyreuther, M., Barsch, R., Krischer, L., Megies, T., Behr, Y., and Wassermann, J.: ObsPy: A Python toolbox for seismology, *Seismol. Res. Lett.*, 81, 530–533, 2010.
- Bhargavi, M. and Gowda, S. D.: A novel validity index with dynamic cut-off for determining true clusters, *Pattern Recogn.*, 48, 3673–3687, 2015.
- Bindschadler, R., Vornberger, P. L., and Shabtaie, S.: The detailed net mass balance of the ice plain on Ice Stream B, Antarctica: a geographic information system approach, *J. Glaciol.*, 39, 471–482, 1993.
- Bindschadler, R., Vornberger, P., and Gray, L.: Changes in the ice plain of Whillans Ice Stream, West Antarctica, *J. Glaciol.*, 51, 620–636, 2005.
- Bougamont, M., Tulaczyk, S., and Joughin, I.: Numerical investigations of the slow-down of Whillans Ice Stream, West Antarctica: is it shutting down like Ice Stream C?, *Ann. Glaciol.*, 37, 239–246, 2003.
- Bouveyron, C., Girard, S., and Schmid, C.: High-dimensional data clustering, *Comput. Stat. Data An.*, 52, 502–519, 2007.
- Breiman, L.: Random forests, *Mach. Learn.*, 45, 5–32, 2001.
- Burton-Johnson, A., Black, M., Fretwell, P. T., and Kaluza-Gilbert, J.: An automated methodology for differentiating rock from snow, clouds and sea in Antarctica from Landsat 8 imagery: a new rock outcrop map and area estimation for the entire Antarctic continent, *The Cryosphere*, 10, 1665–1677, <https://doi.org/10.5194/tc-10-1665-2016>, 2016.
- Campbell, A. J., Hulbe, C. L., and Lee, C.-K.: Ice stream slowdown will drive long-term thinning of the Ross ice shelf, with or without ocean warming, *Geophys. Res. Lett.*, 45, 201–206, 2018.
- Carmichael, J. D., Pettit, E. C., Hoffman, M., Fountain, A., and Hallet, B.: Seismic multiplet response triggered by melt at Blood Falls, Taylor Glacier, Antarctica, *J. Geophys. Res.-Earth Surf.*, 117, F03004, <https://doi.org/10.1029/2011JF002221>, 2012.
- Caruana, R. and Niculescu-Mizil, A.: An empirical comparison of supervised learning algorithms, in: Proceedings of the 23rd international conference on Machine learning, 25–29 June 2006, Pittsburgh Pennsylvania USA, 161–168, 2006.
- Chamarczuk, M., Nishitsuji, Y., Malinowski, M., and Draganov, D.: Unsupervised learning used in automatic detection and classification of ambient-noise recordings from a large-N array, *Seismol. Res. Lett.*, 91, 370–389, 2020.
- Chaput, J., Aster, R. C., McGrath, D., Baker, M., Anthony, R. E., Gerstoft, P., Bromirski, P., Nyblade, A., Stephen, R. A., Wiens, D. A., et al.: Near-Surface Environmentally Forced Changes in the Ross Ice Shelf Observed With Ambient Seismic Noise, *Geophys. Res. Lett.*, 45, 11–187, 2018.
- Chen, Z., Bromirski, P., Gerstoft, P., Stephen, R., Lee, W. S., Yun, S., Olinger, S., Aster, R., Wiens, D., and Nyblade, A.: Ross Ice Shelf icequakes associated with ocean gravity wave activity, *Geophys. Res. Lett.*, 46, 8893–8902, 2019.

- Cole, H. M.: Tidally Induced Seismicity at the Grounded Margins of the Ross Ice Shelf, Antarctica, Ph.D. thesis, Colorado State University, 2020.
- Colgan, W., Rajaram, H., Abdalati, W., McCutchan, C., Mottram, R., Moussavi, M. S., and Grigsby, S.: Glacier crevasses: Observations, models, and mass balance implications, *Rev. Geophys.*, 54, 119–161, 2016.
- Cracknell, M. J. and Reading, A. M.: The upside of uncertainty: Identification of lithology contact zones from airborne geophysics and satellite data using random forests and support vector machines, *Geophysics*, 78, WB113–WB126, 2013.
- Demartines, P. and Hérault, J.: Curvilinear component analysis: A self-organizing neural network for nonlinear mapping of data sets, *IEEE T. Neural Netw.*, 8, 148–154, 1997.
- Ekström, G., Nettles, M., and Abers, G. A.: Glacial earthquakes, *Science*, 302, 622–624, 2003.
- Erofeeva, L., Padman, L., and Howard, S. L.: Tide Model Driver (TMD) version 2.5, Toolbox for Matlab 2020, GitHub [code], [https://www.github.com/EarthAndSpaceResearch/TMD\\_Matlab\\_Toolbox\\_v2.5](https://www.github.com/EarthAndSpaceResearch/TMD_Matlab_Toolbox_v2.5) (last access: 18 March 2024), 2020.
- Famili, A. F., Liu, G., and Liu, Z.: Evaluation and optimization of clustering in gene expression data analysis, *Bioinformatics*, 20, 1535–1545, 2004.
- Fountain, A. G. and Walder, J. S.: Water flow through temperate glaciers, *Rev. Geophys.*, 36, 299–328, 1998.
- Galvis, I. S., Villa, Y., Duarte, C., Sierra, D., and Agudelo, W.: Seismic attribute selection and clustering to detect and classify surface waves in multicomponent seismic data by using k-means algorithm, *The Leading Edge*, 36, 239–248, 2017.
- George, A.: Efficient high dimension data clustering using constraint-partitioning k-means algorithm., *Int. Arab J. Inf. Technol.*, 10, 467–476, 2013.
- Glynn, C. and Naylor, P.: GeoDataViz-Toolkit, GitHub [code], <https://github.com/OrdnanceSurvey/GeoDataViz-Toolkit> (last access: 18 March 2024), 2021.
- Hammer, C., Ohrnberger, M., and Schlindwein, V.: Pattern of cryospheric seismic events observed at Ekström Ice Shelf, Antarctica, *Geophys. Res. Lett.*, 42, 3936–3943, 2015.
- Hardy, A.: On the number of clusters, *Comput. Stat. Data An.*, 23, 83–96, 1996.
- He, Z. and Yu, C.: Clustering stability-based evolutionary k-means, *Soft Comput.*, 23, 305–321, 2019.
- Heck, M., Hammer, C., van Herwijnen, A., Schweizer, J., and Fäh, D.: Automatic detection of snow avalanches in continuous seismic data using hidden Markov models, *Nat. Hazards Earth Syst. Sci.*, 18, 383–396, <https://doi.org/10.5194/nhess-18-383-2018>, 2018.
- Helmstetter, A., Moreau, L., Nicolas, B., Comon, P., and Gay, M.: Intermediate-depth icequakes and harmonic tremor in an Alpine glacier (Glacier d’Argentière, France): Evidence for hydraulic fracturing?, *J. Geophys. Res.-Earth Surf.*, 120, 402–416, 2015.
- Hibert, C., Michéa, D., Provost, F., Malet, J., and Geertsema, M.: Exploration of continuous seismic recordings with a machine learning approach to document 20 yr of landslide activity in Alaska, *Geophys. J. Int.*, 219, 1138–1147, 2019.
- Hotelling, H.: Analysis of a complex of statistical variables into principal components, *J. Educ. Psychol.*, 24, 417, <https://doi.org/10.1037/h0071325>, 1933.
- Howard, S. L., Erofeeva, S., and Padman, L.: CATS2008: Circum-Antarctic Tidal Simulation version 2008, U.S. Antarctic Program (USAP) Data Center [data set], <https://doi.org/10.15784/601235>, 2019.
- Hudson, T. S., Brisbourne, A. M., White, R. S., Kendall, J.-M., Arthern, R., and Smith, A. M.: Breaking the ice: Identifying hydraulically forced crevassing, *Geophys. Res. Lett.*, 47, e2020GL090597, <https://doi.org/10.1029/2020GL090597>, 2020.
- Jain, A. K.: Data clustering: 50 years beyond K-means, *Pattern Recogn. Lett.*, 31, 651–666, 2010.
- Jain, A. K. and Dubes, R. C.: Algorithms for clustering data, Prentice-Hall, Inc., 1988.
- Jenkins, W. F., Gerstoft, P., Bianco, M. J., and Bromirski, P. D.: Unsupervised deep clustering of seismic data: Monitoring the Ross Ice Shelf, Antarctica, *J. Geophys. Res.-Sol. Ea.*, 126, e2021JB021716, <https://doi.org/10.1029/2021JB021716>, 2021.
- Johnson, C. W., Ben-Zion, Y., Meng, H., and Vernon, F.: Identifying different classes of seismic noise signals using unsupervised learning, *Geophys. Res. Lett.*, 47, e2020GL088353, <https://doi.org/10.1029/2020GL088353>, 2020.
- Joughin, I., Tulaczyk, S., Bindschadler, R., and Price, S. F.: Changes in West Antarctic ice stream velocities: observation and analysis, *J. Geophys. Res.-Sol. Ea.*, 107, EPM–3, <https://doi.org/10.1029/2001JB001029>, 2002.
- Kanao, M.: A New Trend in Cryoseismology: A Proxy for Detecting the Polar Surface Environment, *Polar Seismology: Advances and Impact*, p. 75, 2018.
- Köhler, A., Ohrnberger, M., and Scherbaum, F.: Unsupervised pattern recognition in continuous seismic wavefield records using self-organizing maps, *Geophys. J. Int.*, 182, 1619–1630, 2010.
- Köhler, A., Chapuis, A., Nuth, C., Kohler, J., and Weidle, C.: Autonomous detection of calving-related seismicity at Kronebreen, Svalbard, *The Cryosphere*, 6, 393–406, <https://doi.org/10.5194/tc-6-393-2012>, 2012.
- Krischer, L., Megies, T., Barsch, R., Beyreuther, M., Lecocq, T., Caudron, C., and Wassermann, J.: ObsPy: A bridge for seismology into the scientific Python ecosystem, *Comput. Sci. Discov.*, 8, 014003, <https://doi.org/10.1088/1749-4699/8/1/014003>, 2015.
- Latto, B.: beccalatto/multi\_sta\_lta: Towards the systematic reconnaissance of seismic signals from glaciers and ice sheets – Part 1: Event detection for cryoseismology (v1.0.0), Zenodo [code], <https://doi.org/10.5281/zenodo.11062070>, 2024.
- Latto, R. B., Turner, R. J., Reading, A. M., and Winberry, J. P.: Towards the systematic reconnaissance of seismic signals from glaciers and ice sheets – Part 1: Event detection for cryoseismology, *The Cryosphere*, 18, 2061–2079, <https://doi.org/10.5194/tc-18-2061-2024>, 2024.
- Legany, C., Juhasz, S., and Babos, A.: Cluster validity measurement techniques, in: Proceedings of the 5th WSEAS international conference on artificial intelligence, knowledge engineering and data bases, 388–393, World Scientific and Engineering Academy and Society (WSEAS) Stevens Point, 15–17 February 2006, Madrid Spain, edited by: Lopez Espi, P. L., Giron-Sierra, J. M., Drigas, A. S., World Scientific and Engineering Academy and Society (WSEAS) Stevens Point, Wisconsin, United States, ISBN 1112222339, 2006.
- Lombardi, D., Gorodetskaya, I., Barruol, G., and Camelbeeck, T.: Thermally induced icequakes detected on blue ice areas of the East Antarctic ice sheet, *Ann. Glaciol.*, 60, 45–56, 2019.

- MacAyeal, D. R., Banwell, A. F., Okal, E. A., Lin, J., Willis, I. C., Goodsell, B., and MacDonald, G. J.: Diurnal seismicity cycle linked to subsurface melting on an ice shelf, *Ann. Glaciol.*, 60, 137–157, 2019.
- Marsland, S.: Machine learning: an algorithmic perspective, CRC press, Chapman and Hall/CRC, <https://doi.org/10.1201/9781420067194>, 2015.
- McInnes, L., Healy, J., and Melville, J.: Umap: Uniform manifold approximation and projection for dimension reduction, arXiv [preprint], arXiv:1802.03426, 2018.
- Megies, T., Beyreuther, M., Barsch, R., Krischer, L., and Wassermann, J.: ObsPy – What can it do for data centers and observatories?, *Ann. Geophys.*, 54, 47–58, 2011.
- Meilă, M.: The uniqueness of a good optimum for k-means, in: Proceedings of the 23rd international conference on Machine learning, 25–29 June 2006, Pittsburgh, Pennsylvania, USA, ISBN 978-1-59593-383-6, 625–632, 2006.
- Minowa, M., Podolskiy, E. A., and Sugiyama, S.: Tide-modulated ice motion and seismicity of a floating glacier tongue in East Antarctica, *Ann. Glaciol.*, 60, 57–67, <https://doi.org/10.1017/aog.2019.25>, 2019.
- Mohamad, I. B. and Usman, D.: Standardization and its effects on K-means clustering algorithm, *Research Journal of Applied Sciences, Engineering and Technology*, 6, 3299–3303, 2013.
- Mouginot, J., Rignot, E., , and Scheuchl, B.: MEASURES Antarctic Boundaries for IPY 2007-2009 from Satellite Radar, Version 2, Boulder, Colorado, USA, <https://doi.org/10.5067/AXE4121732AD>, 2017.
- Mousavi, S. M., Horton, S. P., Langston, C. A., and Samei, B.: Seismic features and automatic discrimination of deep and shallow induced-microearthquakes using neural network and logistic regression, *Geophys. J. Int.*, 207, 29–46, 2016.
- Mousavi, S. M., Sheng, Y., Zhu, W., and Beroza, G. C.: STanford EArthquake Dataset (STEAD): A global data set of seismic signals for AI, *IEEE Access*, 7, 179464–179476, 2019.
- Nath, P. and Vaughan, D.: Subsurface crevasse formation in glaciers and ice sheets, *J. Geophys. Res.-Sol. Ea.*, 108, ECV–7, <https://doi.org/10.1029/2001JB000453>, 2003.
- Padman, L., Fricker, H. A., Coleman, R., Howard, S., and Erofeeva, L.: A new tide model for the Antarctic ice shelves and seas, *Ann. Glaciol.*, 34, 247–254, 2002.
- Pedregosa, F., Varoquaux, G., Gramfort, A., Michel, V., Thirion, B., Grisel, O., Blondel, M., Prettenhofer, P., Weiss, R., Dubourg, V., Vanderplas, J., Passos, A., Cournapeau, D., Brucher, M., Perrot, M., and Duchesnay, E.: Scikit-learn: Machine Learning in Python, *J. Mach. Learn. Res.*, 12, 2825–2830, 2011.
- Pérez-Campos, X., Singh, S. K., and Beroza, G. C.: Reconciling teleseismic and regional estimates of seismic energy, *B. Seismol. Soc. Am.*, 93, 2123–2130, 2003.
- Podolskiy, E. A. and Walter, F.: Cryoseismology, *Rev. Geophys.*, 54, 708–758, 2016.
- Podolskiy, E. A., Sugiyama, S., Funk, M., Walter, F., Genco, R., Tsutaki, S., Minowa, M., and Ripepe, M.: Tide-modulated ice flow variations drive seismicity near the calving front of Bowdoin Glacier, Greenland, *Geophys. Res. Lett.*, 43, 2036–2044, <https://doi.org/10.1002/2016GL067743>, 2016.
- Podolskiy, E. A., Fujita, K., Sunako, S., Tsushima, A., and Kayastha, R. B.: Nocturnal thermal fracturing of a Himalayan debris-covered glacier revealed by ambient seismic noise, *Geophys. Res. Lett.*, 45, 9699–9709, 2018.
- Podolskiy, E. A., Fujita, K., Sunako, S., and Sato, Y.: Viscoelastic Modeling of Nocturnal Thermal Fracturing in a Himalayan Debris-Covered Glacier, *J. Geophys. Res.-Earth Surf.*, 124, 1485–1515, <https://doi.org/10.1029/2018JF004848>, 2019.
- Pomeroy, J., Brisbourne, A., Evans, J., and Graham, D.: The search for seismic signatures of movement at the glacier bed in a polythermal valley glacier, *Ann. Glaciol.*, 54, 149–156, 2013.
- Pratt, M. J., Winberry, J. P., Wiens, D. A., Anandakrishnan, S., and Alley, R. B.: Seismic and geodetic evidence for grounding-line control of Whillans Ice Stream stick-slip events, *J. Geophys. Res.-Earth Surf.*, 119, 333–348, <https://doi.org/10.1002/2013JF002842>, 2014.
- Price, S. F., Bindshadler, R., Hulbe, C. L., and Joughin, I. R.: Post-stagnation behavior in the upstream regions of Ice Stream C, West Antarctica, *J. Glaciol.*, 47, 283–294, 2001.
- Provost, F., Hibert, C., and Malet, J.-P.: Automatic classification of endogenous landslide seismicity using the Random Forest supervised classifier, *Geophys. Res. Lett.*, 44, 113–120, 2017.
- Retzlaff, R. and Bentley, C. R.: Timing of stagnation of Ice Stream C, West Antarctica, from short-pulse radar studies of buried surface crevasses, *J. Glaciol.*, 39, 553–561, 1993.
- Reynen, A. and Audet, P.: Supervised machine learning on a network scale: Application to seismic event classification and detection, *Geophys. J. Int.*, 210, 1394–1409, 2017.
- Riggelsen, C. and Ohrnberger, M.: A machine learning approach for improving the detection capabilities at 3C seismic stations, *Pure Appl. Geophys.*, 171, 395–411, 2014.
- Rignot, E., Mouginot, J., and Scheuchl, B.: Ice Flow of the Antarctic Ice Sheet, *Science*, 333, 1427–1430, <https://doi.org/10.1126/science.1208336>, 2011.
- Rignot, E., Jacobs, S., Mouginot, J., and Scheuchl, B.: Ice-shelf melting around Antarctica, *Science*, 341, 266–270, 2013.
- Röösli, C., Walter, F., Husen, S., Andrews, L. C., Lüthi, M. P., Catania, G. A., and Kissling, E.: Sustained seismic tremors and icequakes detected in the ablation zone of the Greenland ice sheet, *J. Glaciol.*, 60, 563–575, 2014.
- Rousseeuw, P. J.: Silhouettes: a graphical aid to the interpretation and validation of cluster analysis, *J. Comput. Appl. Math.*, 20, 53–65, 1987.
- Sawi, T., Holtzman, B., Walter, F., and Paisley, J.: An Unsupervised Machine-Learning Approach to Understanding Seismicity at an Alpine Glacier, *J. Geophys. Res.-Earth Surf.*, 127, e2022JF006909, <https://doi.org/10.1029/2022JF006909>, 2022.
- Seydoux, L., Balestrero, R., Poli, P., De Hoop, M., Campillo, M., and Baraniuk, R.: Clustering earthquake signals and background noises in continuous seismic data with unsupervised deep learning, *Nat. Commun.*, 11, 1–12, 2020.
- Sibi, P., Jones, S. A., and Siddarth, P.: Analysis of different activation functions using back propagation neural networks, *J. Theor. Appl. Inf. Technol.*, 47, 1264–1268, 2013.
- Stål, T. and Reading, A. M.: A grid for multidimensional and multivariate spatial representation and data processing, *J. Open Res. Softw.*, 8, 1–10, <https://doi.org/10.5334/JORS.287>, 2020.
- Trebuňa, P., Halčinová, J., Fil'o, M., and Markovič, J.: The importance of normalization and standardization in the process of clustering, in: 2014 IEEE 12th International Symposium on Applied

- Machine Intelligence and Informatics (SAMI), 381–385, IEEE, 2014.
- Tulaczyk, S., Kamb, W. B., and Engelhardt, H. F.: Basal mechanics of ice stream B, West Antarctica: 1. Till mechanics, *J. Geophys. Res.-Sol. Ea.*, 105, 463–481, 2000.
- Turner, R. J., Latto, R. B., and Reading, A. M.: An ObsPy library for event detection and seismic attribute calculation: preparing waveforms for automated analysis, *J. Open Res. Softw.*, 9, 29, <https://doi.org/10.5334/jors.365>, 2021 (code available at: [https://github.com/rossjturner/seismic\\_attributes](https://github.com/rossjturner/seismic_attributes), last access: 18 March 2024).
- Turner, R. J., Latto, R. B., and Reading, A. M.: An ObsPy library for event detection and seismic attribute calculation: preparing waveforms for automated analysis (v1.0.3.post1), Zenodo [code], <https://doi.org/10.5281/zenodo.5499909>, 2021.
- U.S. Geological Survey, E. H. P.: Advanced National Seismic System (ANSS) Comprehensive Catalog of Earthquake Events and Products, <https://doi.org/10.5066/F7MS3QZH>, 2022.
- Van der Maaten, L. and Hinton, G.: Visualizing data using t-SNE, *J. Mach. Learn. Res.*, 9, 2579–2605, 2008.
- VanWormer, D. and Berg, E.: Seismic Evidence for Glacier Motion, *J. Glaciol.*, 12, 259–265, <https://doi.org/10.3189/S002214300003207X>, 1973.
- Wiens, D., Pratt, M., Aster, R., Nyblade, A., Bromirski, P., Stephen, R., and Gerstoft, P.: Longitudinal seismic waves in the Ross Ice Shelf excited by Whillans Ice Stream stick-slip events, *Geoscience*, 7, 677–681, 2016.
- Wiens, D. A., Anandakrishnan, S., Winberry, J. P., and King, M. A.: Simultaneous teleseismic and geodetic observations of the stick-slip motion of an Antarctic ice stream, *Nature*, 453, 770–774, <https://doi.org/10.1038/nature06990>, 2008.
- Winberry, J. P., Anandakrishnan, S., and Alley, R. B.: Seismic observations of transient subglacial water-flow beneath MacAyeal Ice Stream, West Antarctica, *Geophys. Res. Lett.*, 36, L11502, <https://doi.org/10.1029/2009GL037730>, 2009a.
- Winberry, J. P., Anandakrishnan, S., Alley, R. B., Bindschadler, R. A., and King, M. A.: Basal mechanics of ice streams: Insights from the stick-slip motion of Whillans Ice Stream, West Antarctica, *J. Geophys. Res.-Earth Surf.*, 114, F01016, <https://doi.org/10.1029/2008JF001035>, 2009b.
- Winberry, J. P., Anandakrishnan, S., and Wiens, D.: Geophysical Study of Ice Stream Stick-slip dynamics, International Federation of Digital Seismograph Networks [data set], [https://doi.org/10.7914/SN/2C\\_2010](https://doi.org/10.7914/SN/2C_2010), 2010.
- Winberry, J. P., Anandakrishnan, S., Wiens, D. A., Alley, R. B., and Christianson, K.: Dynamics of stick-slip motion, Whillans Ice Stream, Antarctica, *Earth Planet. Sc. Lett.*, 305, 283–289, 2011.
- Winberry, J. P., Anandakrishnan, S., Wiens, D. A., and Alley, R. B.: Nucleation and seismic tremor associated with the glacial earthquakes of Whillans Ice Stream, Antarctica, *Geophys. Res. Lett.*, 40, 312–315, <https://doi.org/10.1002/grl.50130>, 2013.
- Winberry, J. P., Anandakrishnan, S., Alley, R. B., Wiens, D. A., and Pratt, M. J.: Tidal pacing, skipped slips and the slowdown of Whillans Ice Stream, Antarctica, *J. Glaciol.*, 60, 795–807, 2014.
- Wright, A. and Siegert, M.: A fourth inventory of Antarctic subglacial lakes, *Antarct. Sci.*, 24, 659–664, 2012.
- Yoon, C. E., O'Reilly, O., Bergen, K. J., and Beroza, G. C.: Earthquake detection through computationally efficient similarity search, *Sci. Adv.*, 1, e1501057, <https://doi.org/10.1126/sciadv.1501057>, 2015.
- Zadeh, R. B. and Ben-David, S.: A Uniqueness Theorem for Clustering, in: Proceedings of the Twenty-Fifth Conference on Uncertainty in Artificial Intelligence, UAI '09, 639–646, AUA Press, Arlington, Virginia, USA, ISBN 9780974903958, 2009.
- Zu Eissen, B. and Wißbrock, F.: On cluster validity and the information need of users, ACTA Press, 216–221, 2003.